High Resolution X-ray Tomography in Nuclear Energy Research

Ion Tiseanu, Teddy Craciunescu

National Institute for Lasers

Plasma and Radiation Physics

Bucharest, Romania

tiseanu@infim.ro

OUTLINE

• Contribution to EURATOM FUSION
- Assessment of the Structural Integrity of a Prototypical Instrumented IFMIF High Flux Test Module Rig by Fully 3D X-ray Microtomography
- 3D X-ray Micro-Tomography for Modeling of Nb3Sn Multifilamentary Superconducting Wires
- Neutron emission tomography for limited data set at JET tokamak

• Contribution to EURATOM FISSION
- Nuclear waste management: X-ray micro-tomography for crystalline host rock analysis

• X-ray Tomography for Nuclear Applications and Research
- Ultra fast X-Ray Computed Tomography for Transient Phenomena
- Gamma Emission Tomography

• OUTLOOK

Fan-beam geometry makes use of a linear x-ray detector and a divergent fan beam of x-rays. X-rays that are scattered in the same plane as the detector can be detected, but x-rays that are scattered out of plane miss the linear detector array and are not detected. Scattered radiation accounts for approximately 5% of the signal in typical fan beam scanners.

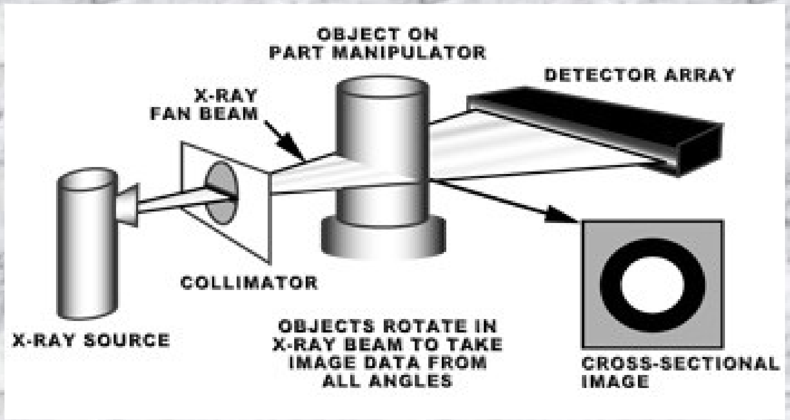

Cone-beam geometry, also known as volume or 3D scanning, is a recently developed technique that can greatly speed up collection of CT data from an object. For relatively large and dense samples cone beam geometries can lead to four detected scatter events for every detected primary photon. This geometry is currently in use in our CT.

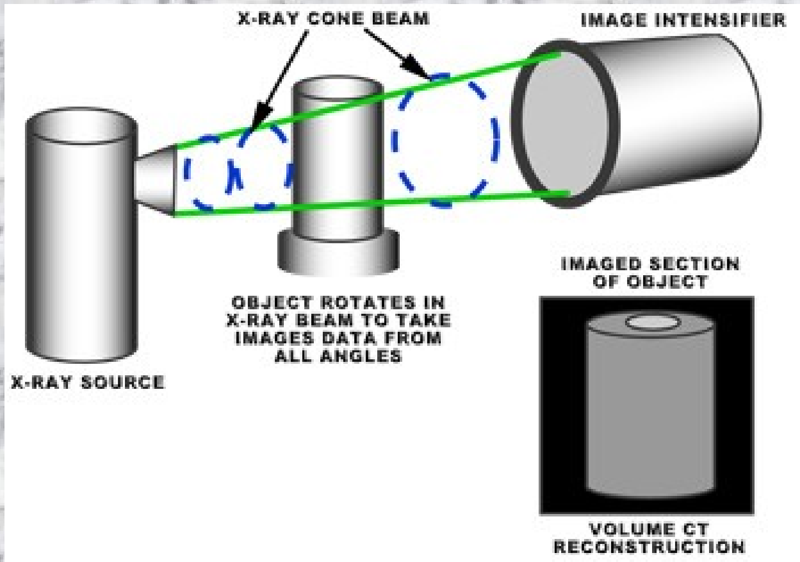

Reconstruction of time-resolved energy spectrum of short-pulsed neutron sources

The neutron flux shape is recorded by a number of detectors placed at various distances from the source.

$$S(T,D) = \int_{t_1}^{t_2} dt \int_{E_1}^{E_2} dE \cdot f_E(t,E)\,\delta\left(t - T + \frac{D}{\sqrt{2E/m_n}}\right)$$

$$T = t + \frac{D}{\sqrt{2E/m}}$$

Transform to tomography:

$$T = t + D \cdot q$$

$$q = 1/v$$

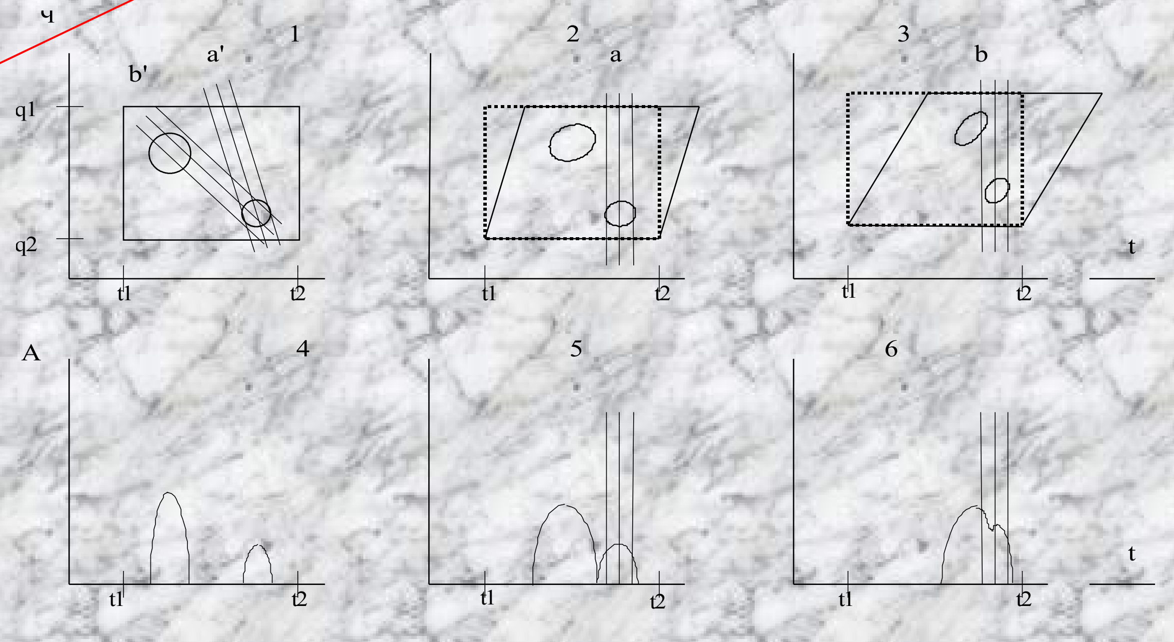

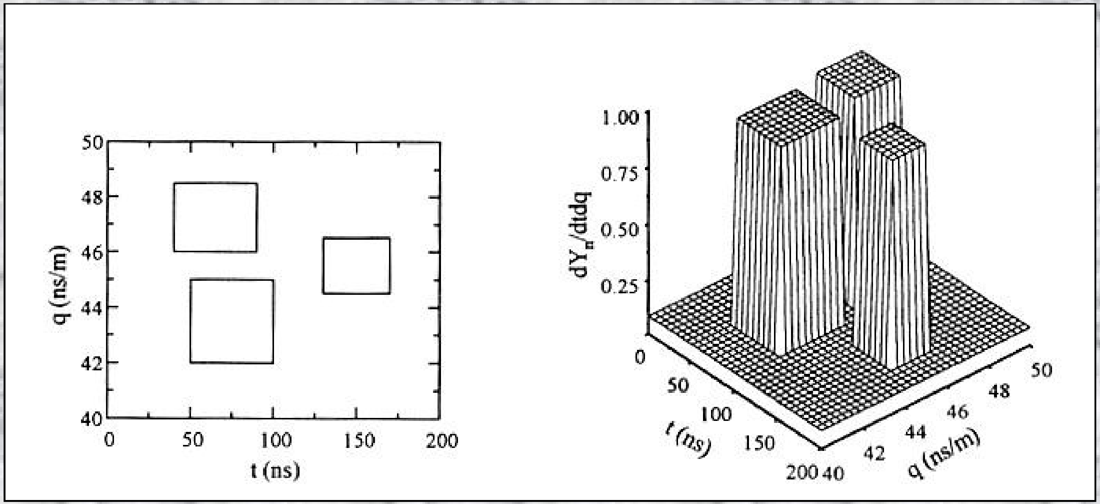

Phantom (test distribution)

- The rectangle shape of the three spikes is used to evaluate the shape distortion inherently caused by the limited view angle domain.

- Equal height of spikes monitor reconstruction with erroneous heights

- The resolution of the shape reconstruction is monitored by the size of the spikes and also by the relative shifts and gaps between spikes.

- A background of 10% of the spike's height is superimposed to appreciate the quality of signal to noise ratio reconstruction

The shape of the phantom simulates both the neutron emission caused by the interaction of an azimuthal or radial deuteron component with the dense plasma target (the two peaks at the beginning of the emission) and by the interaction of an axial deuteron beam with a dense plasma target (the peak in the latter phase of emission).

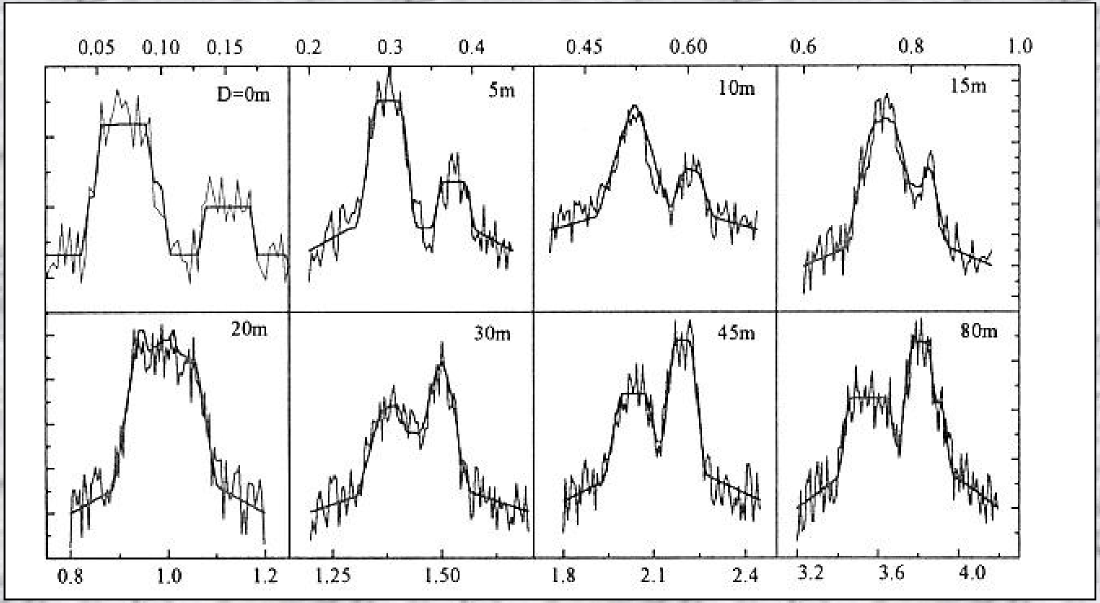

Numerically simulated tomographic projections

Monte Carlo - MC

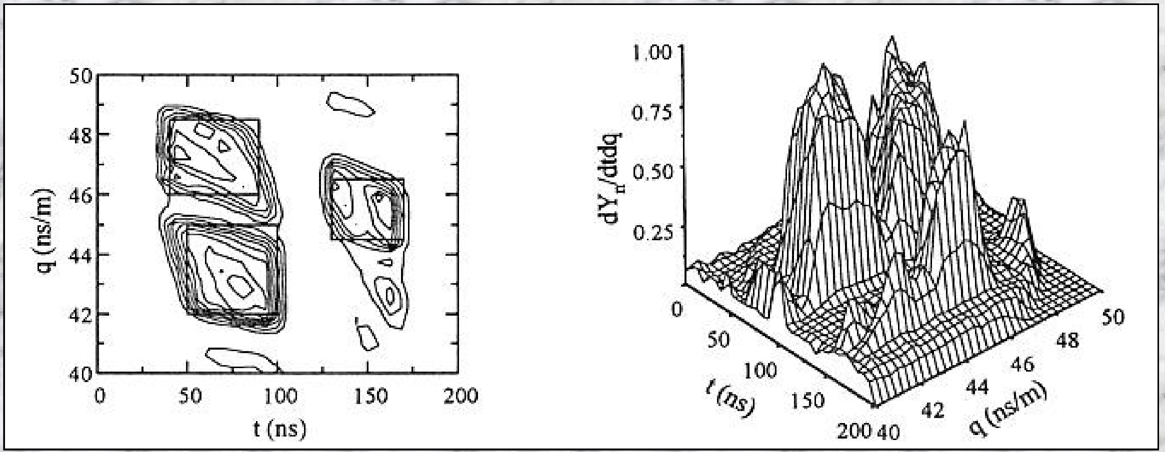

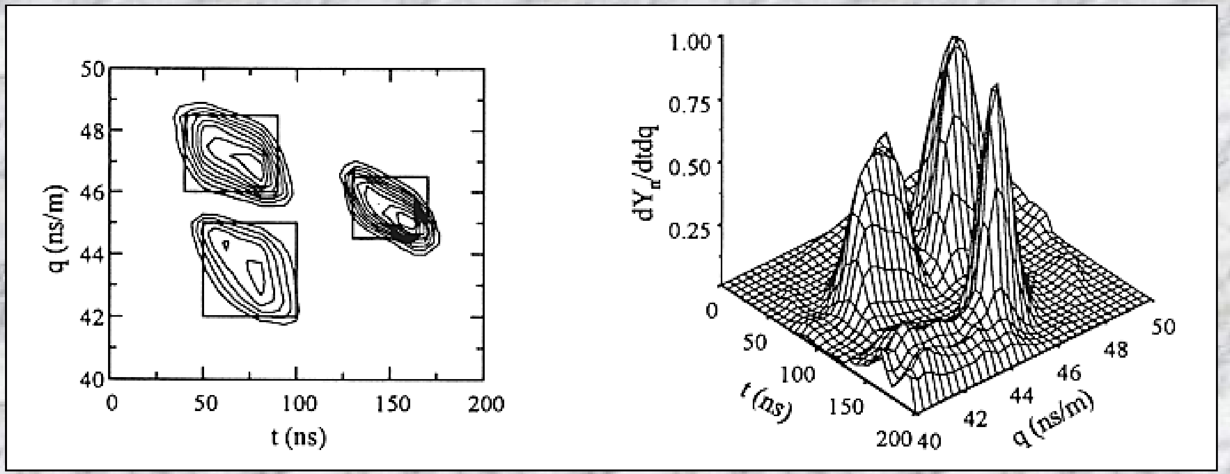

Maximum entropy - ME

Algebraical Reconstruction Technique - ART

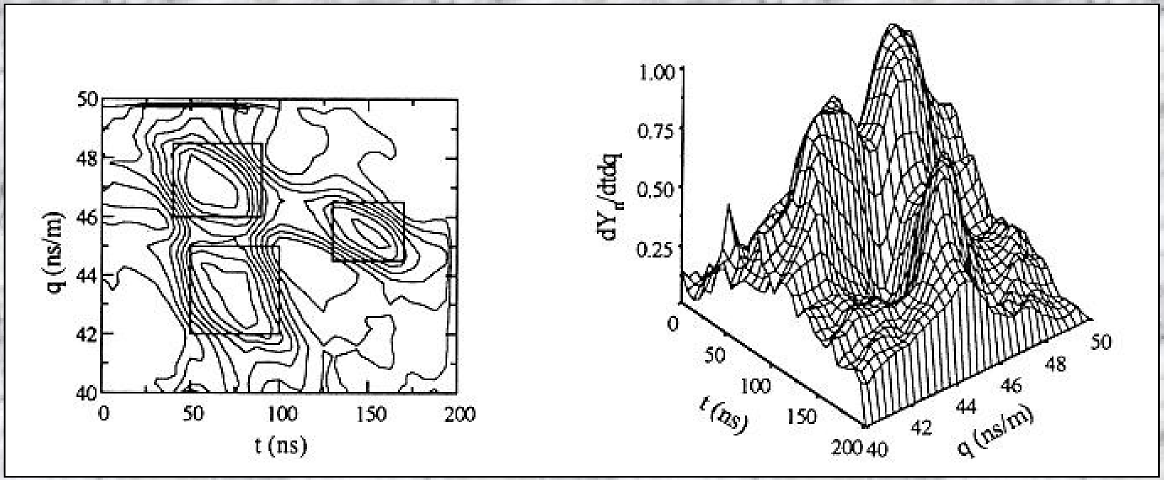

The **SPEED2** operation parameters:

Discharge 8778

• capacitor bank voltage: U=180 kV, W=57 kJ
• deuterium pressures: p=4.25 hPa
• total neutron yield per discharge Yn =2.45 10^10 neutrons;

The time-of-flight diagnostics system: 4 scintillator-photomultiplier detector assemblies placed at distances:

- 1.85 m
- 9.65 m
- 20.15 m
- 29.75 m

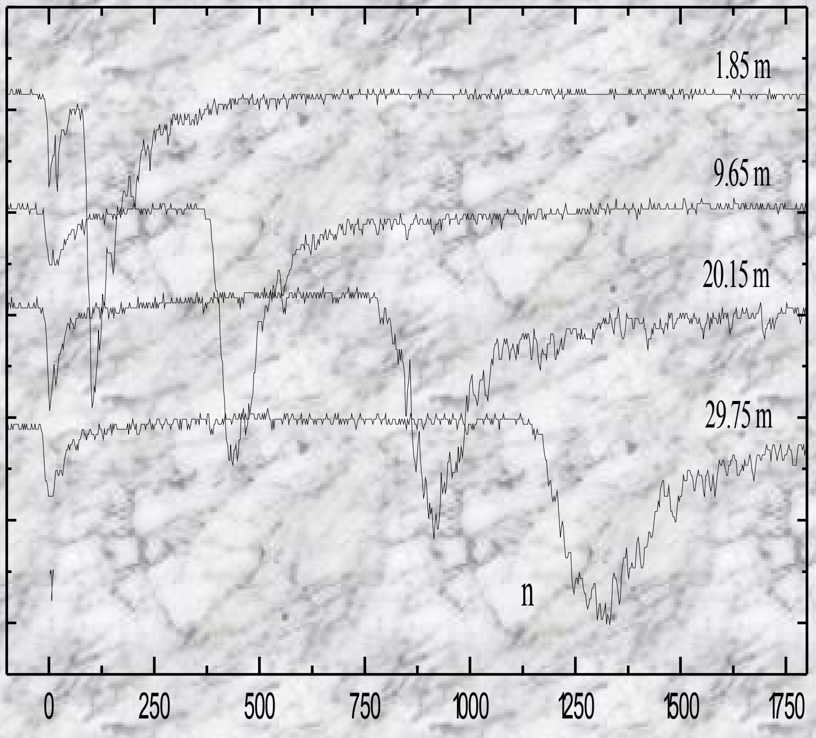

Experimental data
(tomographic projections)

Discharge 8778

Data analysis and interpretation

Superposition of a relatively broad spectrum (700-800 keV full width) with a dominant peak at about 2.5 MeV, arising at about 25-30 ns from the neutron emission start.

Two-component deuteron distribution function (with an average deuteron energy of 100 keV):

-a quasi-axial component (producing the 2.5 MeV peak)

-a radial-azimuthal component (producing the broad spectrum)

Relaxation of the two-component ion distribution by collisions with plasma and background gas $\Rightarrow$ neutron emission in the later part of the pulse

.

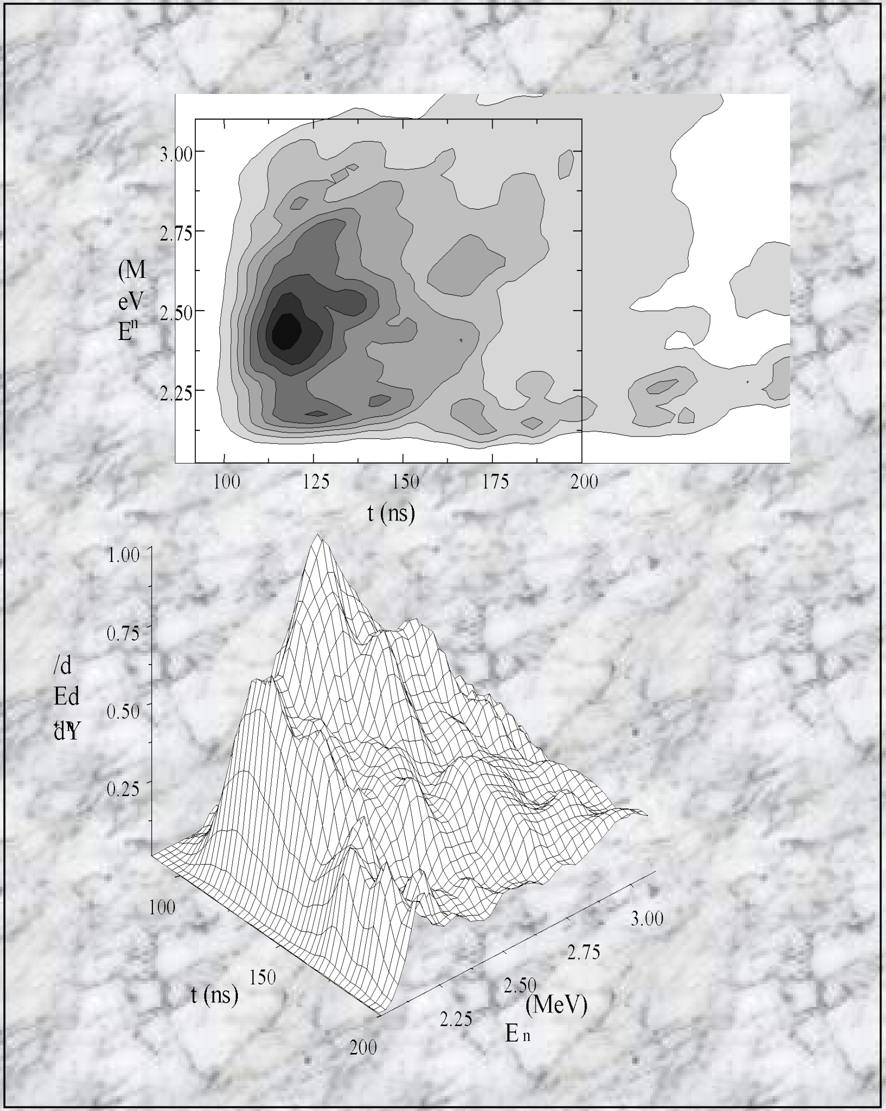

Tomographic reconstruction. The experimental conditions and the numerical procedure provided an energy resolution of 25 keV and a time resolution of 2.5 ns.

X-RAY MICROTOMOGRAPHY FACILITY

Goal:

to provide an universal tool for the NDT analysis of fusion material samples (structural and breeders) before and after various tests (including irradiation).

Applications:

- 3D modelling of miniaturized samples;
- density variations, micro-cracks formation by mechanical/thermal cycling;
- percolation and pore network connectivity in porous materials;
- structural integrity of various components;
- high magnification microradiography for in-situ inspection of samples under mechanical and/or thermal stress.

A computer tomograph is configured to take many views of an object in order to build a three-dimensional (3-D) model of its internal structure. 2-D slices through the object volume can be viewed as images, or the 3-D volume may be rendered, sliced, thresholded and measured directly.

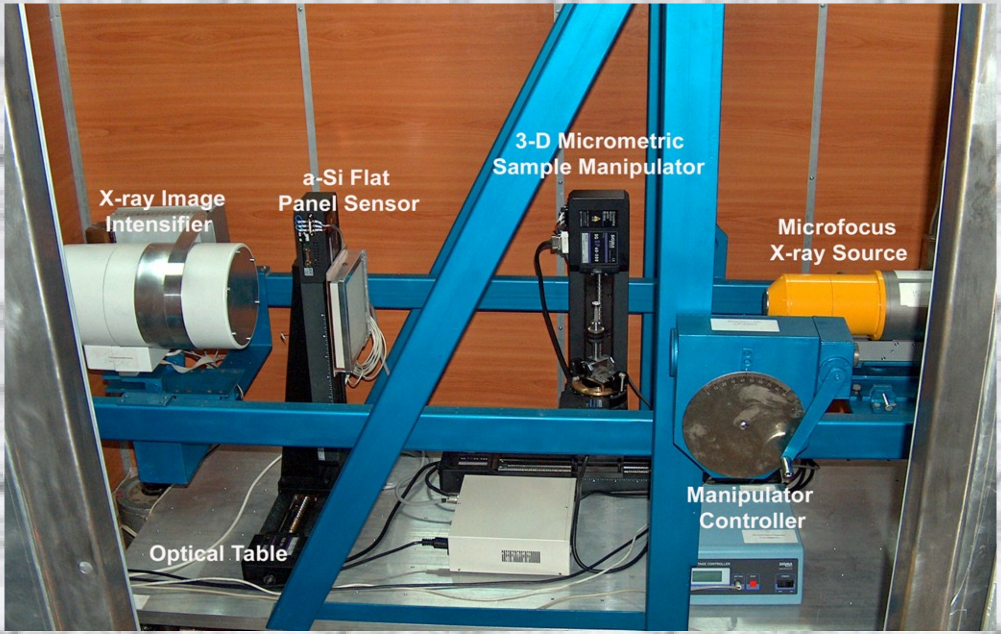

Overall performances

- Magnification < 2000
- Spatial resolution ≅ 5μm
- Density resolution > 0.5%
-3D Reconstruction Time ≅ 2 min. (512x512x512 voxels)
-Probe dimensions: Diameter < 40 mm
Height < 500 mm

The microtomography facility was designed and constructed with European Community support
(EFDA Newsletters: Vol. 2003/2, April 5, 2003 ,Vol. 2003/6 Dec. 2003)

INFLPR UPGRADED X-RAY subMICROTOMOGRAPHY FACILITY

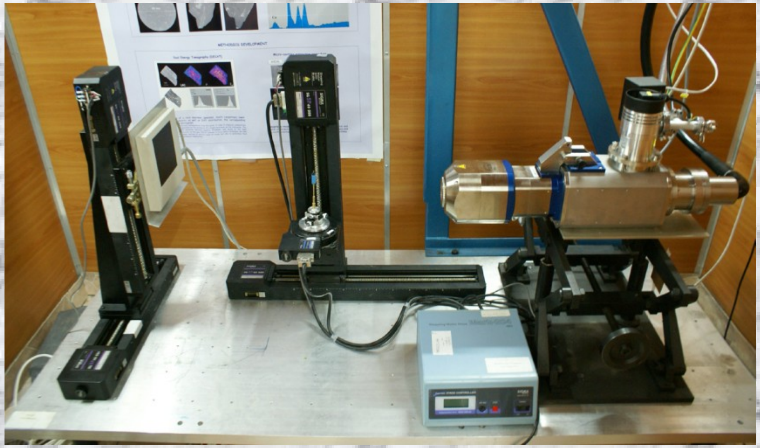

- X-ray source
  - Max. 225 kV
  - **Focus spot <0.8µ**
- Detector
  - a-Si flat panel
  - 1210x1216 pixels
  - 0.1x0.1 mm^2
- High precision six-axis manipulator

HIGH END X-RAY MICROTOMOGRAPHY FACILITY

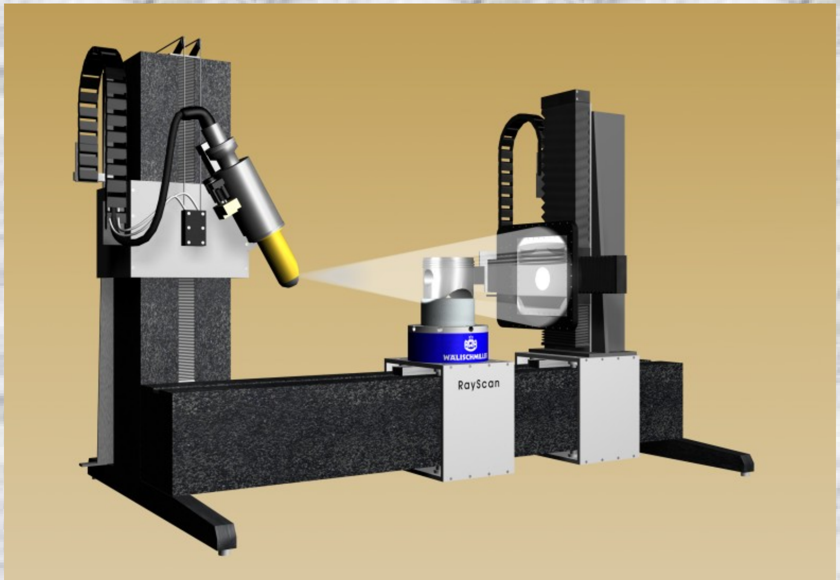

- X-ray source
  - Max. 225 kV
  - Focus spot 5-200µ
- Detector
  - a-Si flat panel
  - **2048x2048 pixels**
  - 0.2x0.2 mm^2
- High precision up to seven-axis manipulator

Advanced Computed Tomography System for the Inspection of Large Aluminium Car Bodies

3D CT of an aluminum laser weld

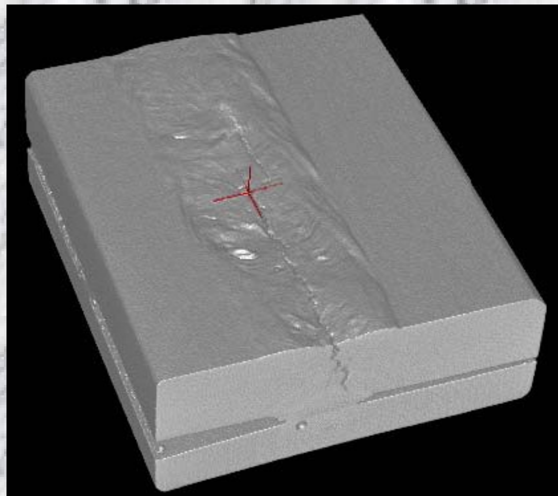

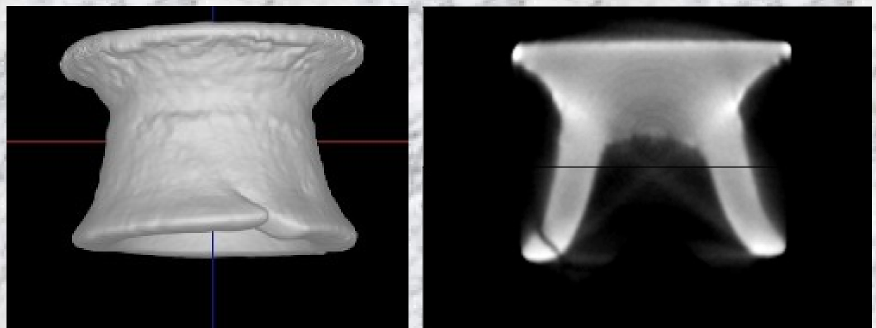

Rivet joint extracted from a car body

Space resolution benchmark (old facility)

Gold foil spiral (foil thickness – 5 µm)

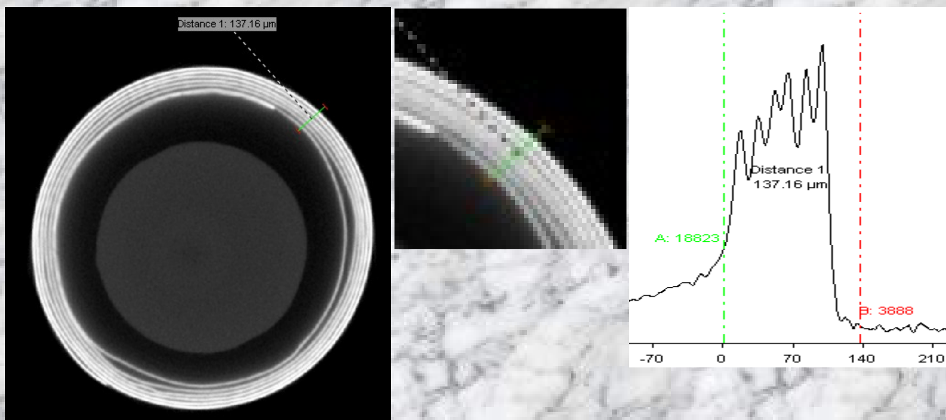

Metallic catalyst sample (thinnest wire – 3 µm)

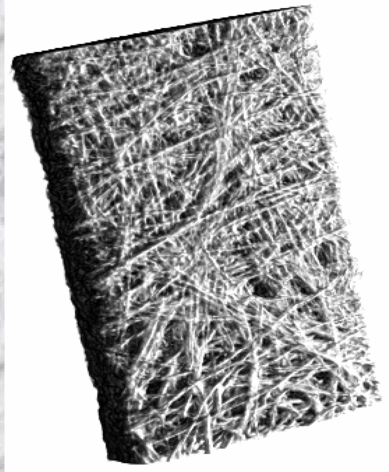

Tomographic reconstruction

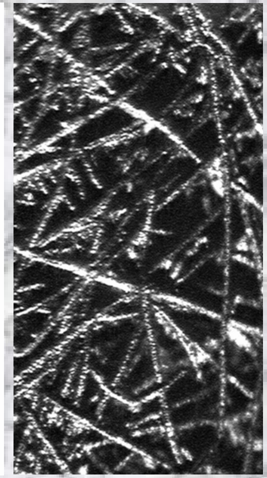

Optical microscopy

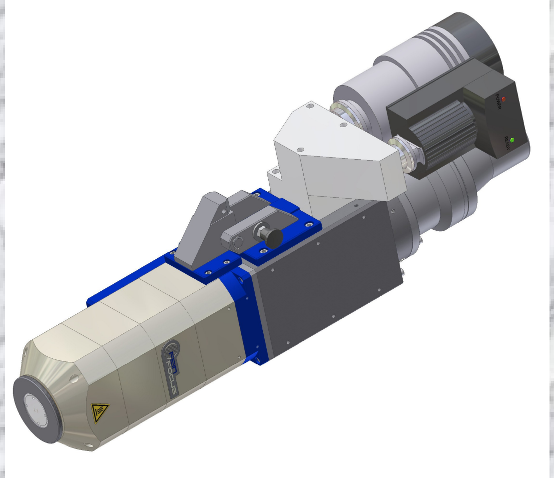

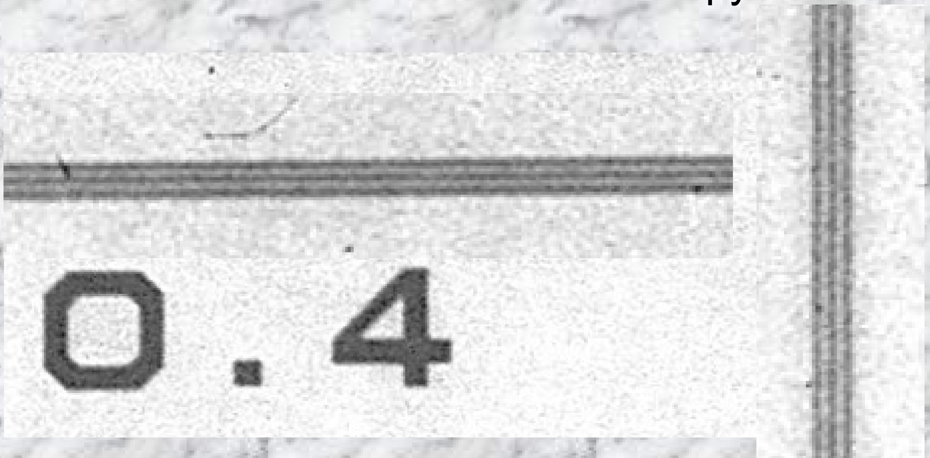

Current facility: Nanofocus tube (<0.4 µm)

X-RAY MICROTOMOGRAPHY of the IFMIF HFTM IRRADIATION CAPSULE

IFMIF - International Fusion Materials Irradiation Facility

3-D tomography of miniaturized samples

Radiography | Density plot | Sagital view

SUS traction probe 2 mm diameter

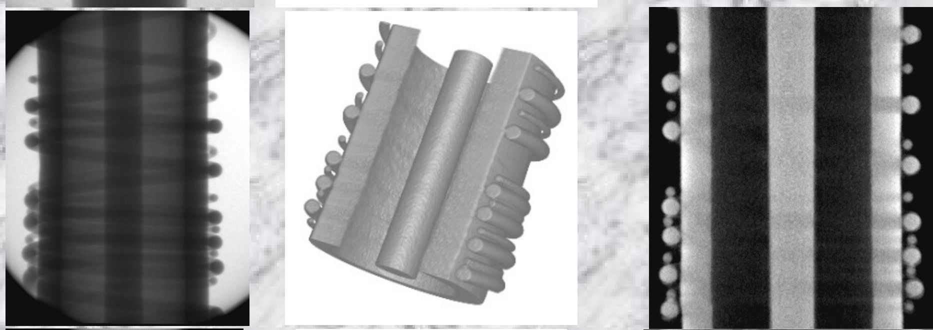

Calibration sample: Cu tube 2.2 mm, Ag central wire 0.5 mm and coiled kanthal wires 0.18 and 0.08 mm

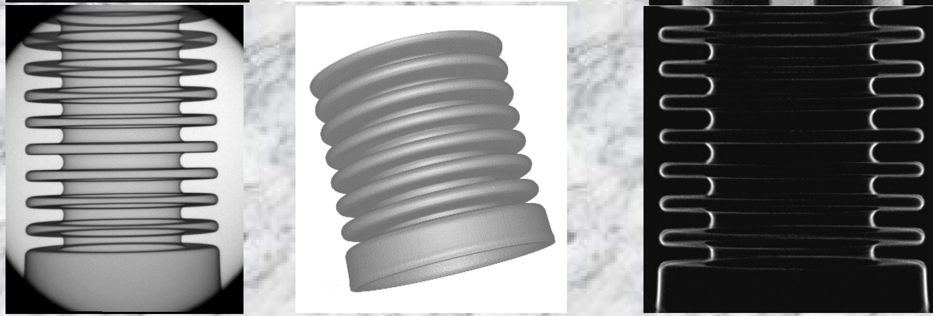

Steel bellows of 6.5 mm

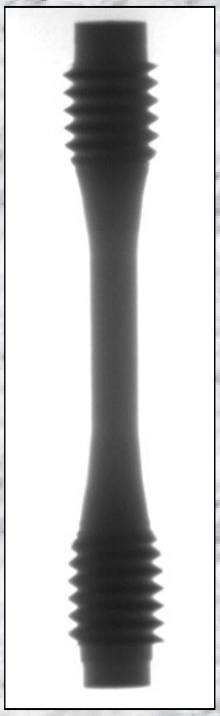

Push-pull fatigue specimen

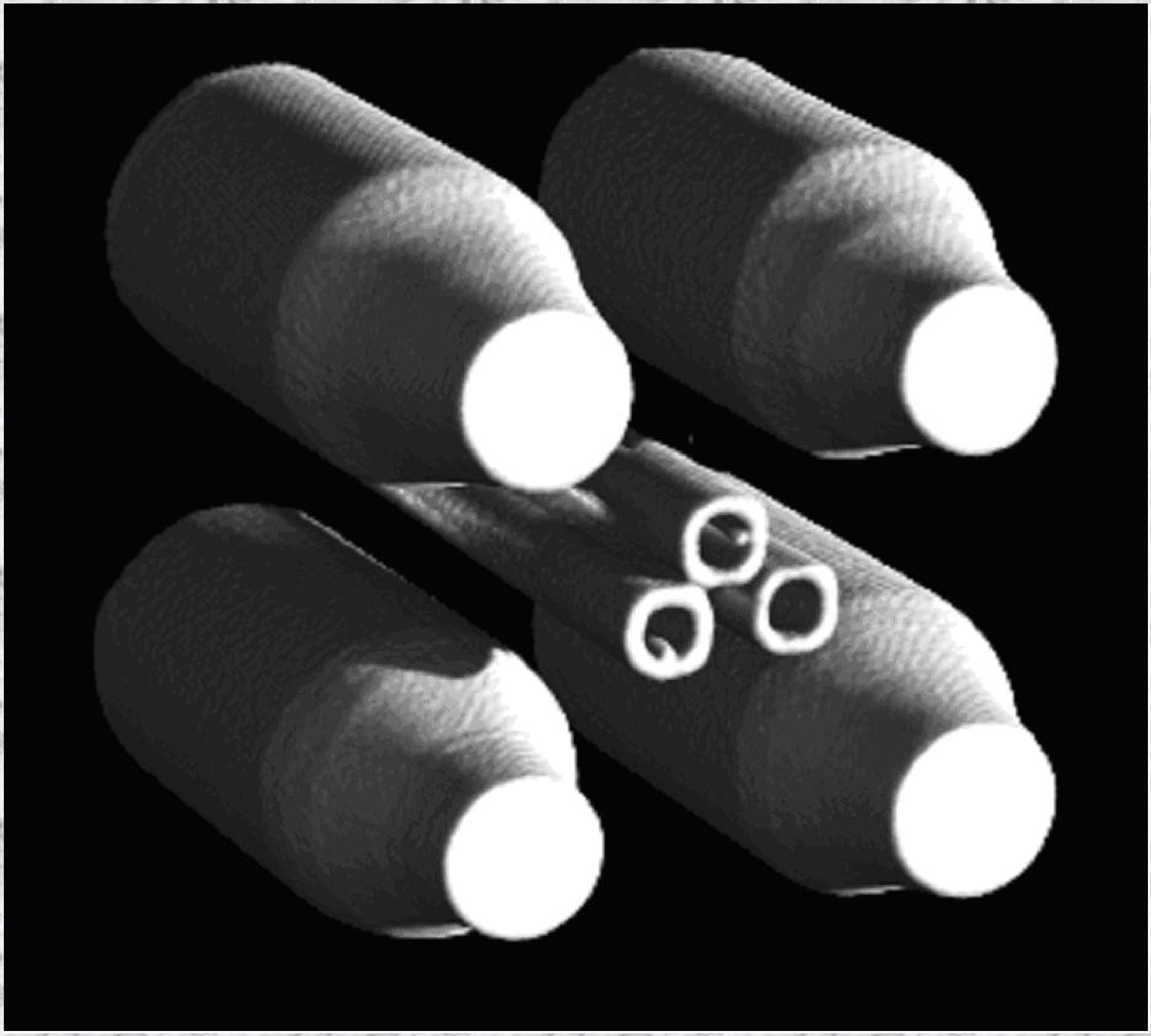

IFMIF - International Fusion Materials Irradiation Facility

Assessment of the structural integrity of a prototypical instrumented IFMIF high flux test module (HFTM) rig by fully 3D X-ray microtomography

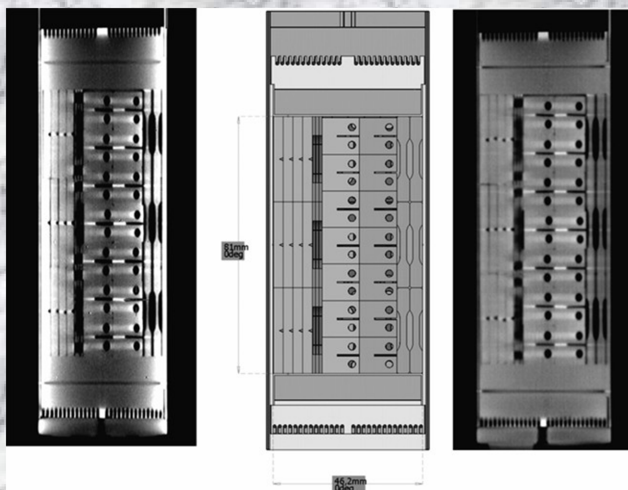

Tomography reconstruction of the HFTM irradiation capsule: longitudinal cross-section (left - microfocus tube, 225 kV, right - 450 kV tube, and middle – a comparison with its CAD model.

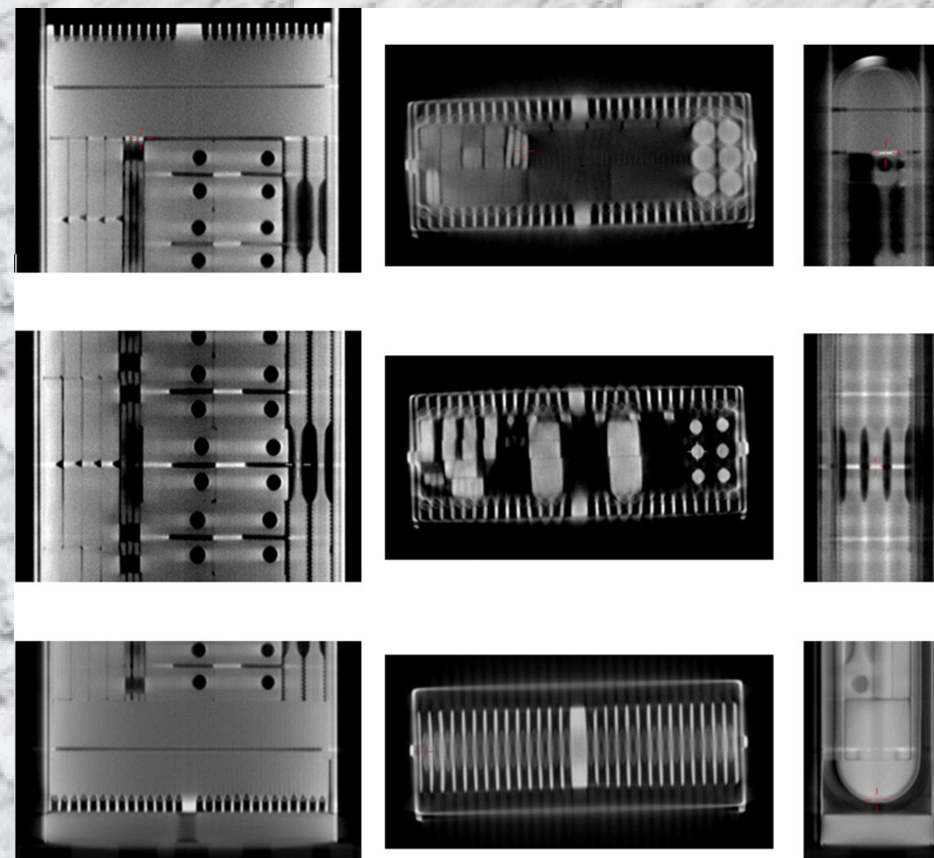

Tomographic reconstruction for optimum combination of the irradiation parameters and enhanced magnification for detail visualization. (microfocus tube, U= 220 kV, voxel size = 60m)

IFMIF - International Fusion Materials Irradiation Facility

Assessment of the structural integrity of a prototypical instrumented IFMIF high flux test module (HFTM) rig by fully 3D X-ray microtomography (con't)

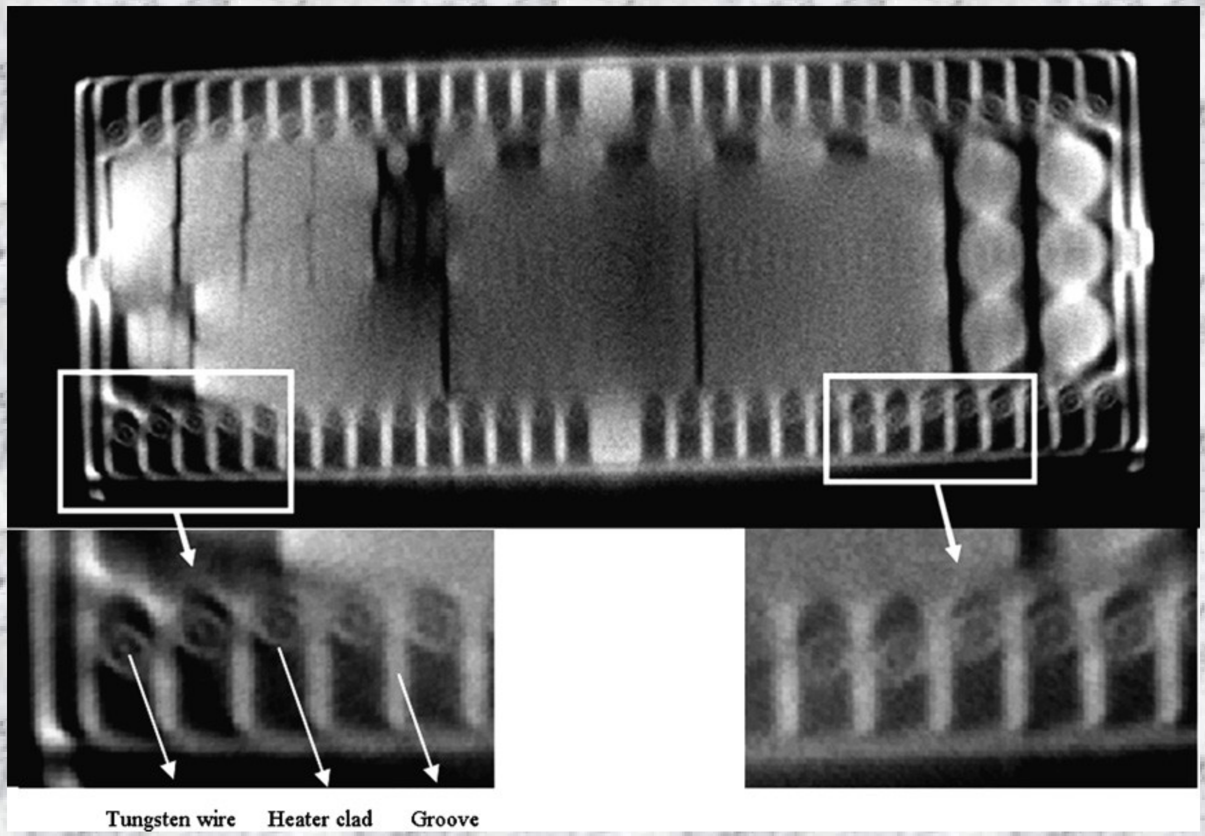

Tomographic cross-section that illustrates the gaps (lack of thermal contact) between the heater coils and the groove channels. Heater diameter approx. 1 mm, tungsten wire 100 microns diameter. Microfocus tube, U= 220 kV, I = 300A, voxel size = 60m

Steel sample with brazed heaters inside – IFMIF HFTM

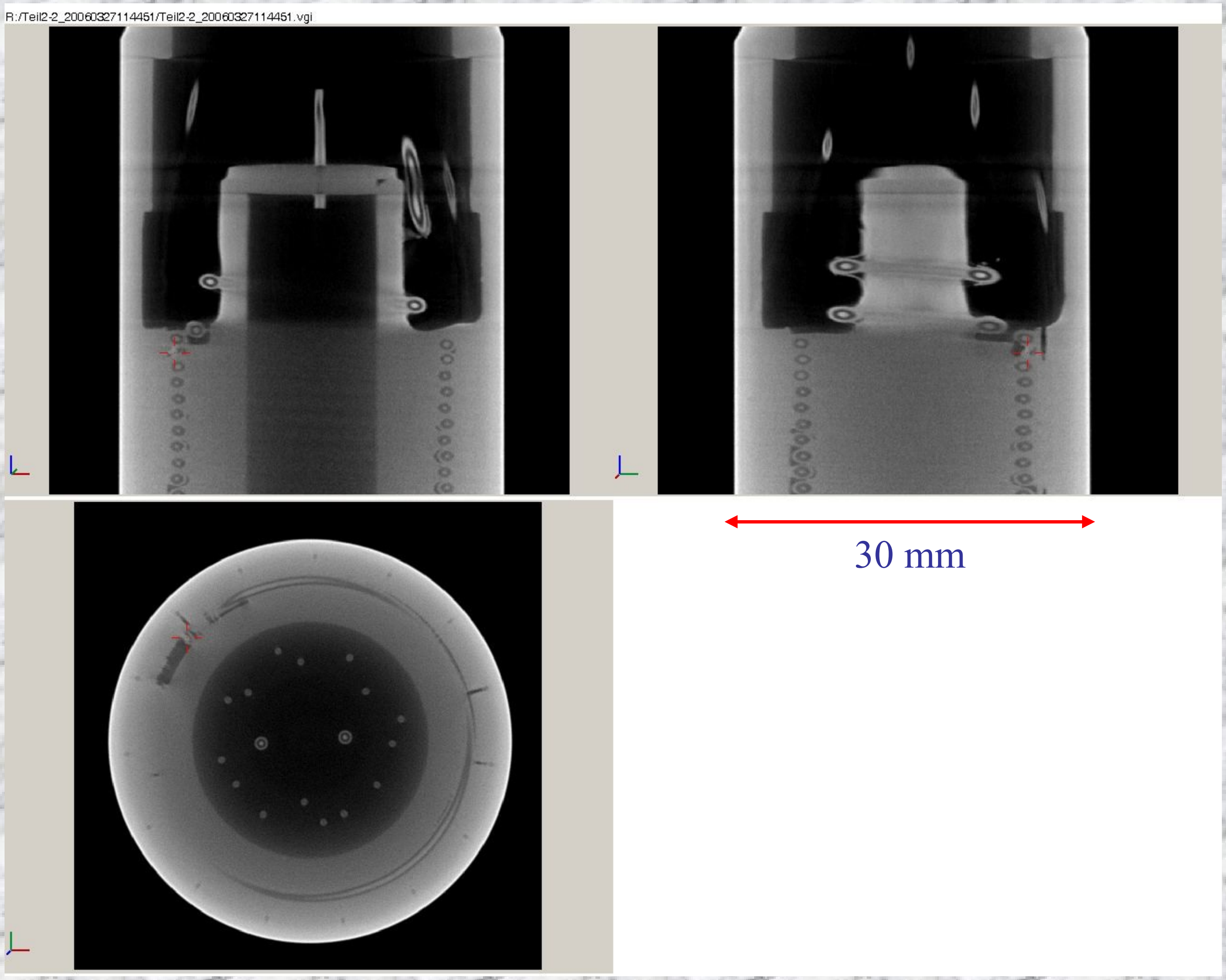

Emission tomography facility for IFMIF irradiated capsules: technical concept

Established by numerical simulations and validated by experimental tests

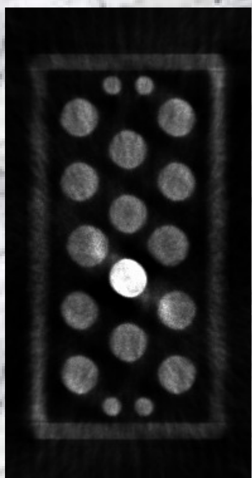

Reconstruction of transversal (left) and longitudinal (bottom) cross-sections of a numerically simulated test capsule

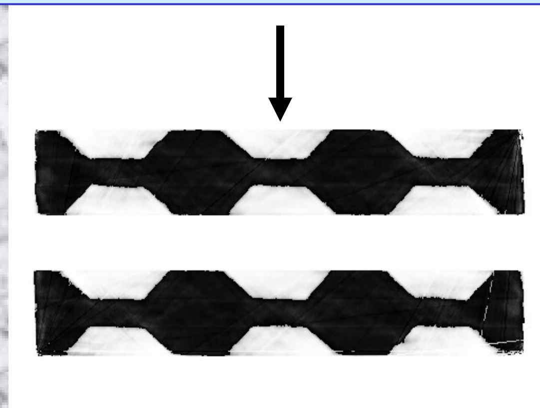

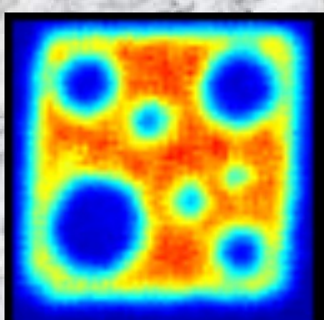

Experimental test phantom (10 x 10 cm Plexiglas with rods surrounded by a volume, non-uniformly filled with ^{131}I liquid solution)

The whole gamma spectroscopy chain and the collimating configuration were accurately described by full 3-D Monte Carlo simulations.

Emission tomography measurement tests were carried out on an adapted gamma-scanning system in the Hot-Cell facility at the Institute for Nuclear Research, Pitesti, Romania.

The samples were selected to simulate the IFMIF irradiation capsule.

Both the simulated and measured tomographic projections were processed within a proprietary reconstruction program based on the criterion of maximum entropy.

The design parameters for space resolution and isotope selectivity are well within reach.

X-RAY MICROTOMOGRAPHY for ITER

ITER- Compressed pebble bed

3-D tomography reconstruction insert: frontal cross-sections of the bottom zone showing pebbles in contact with the steel plate

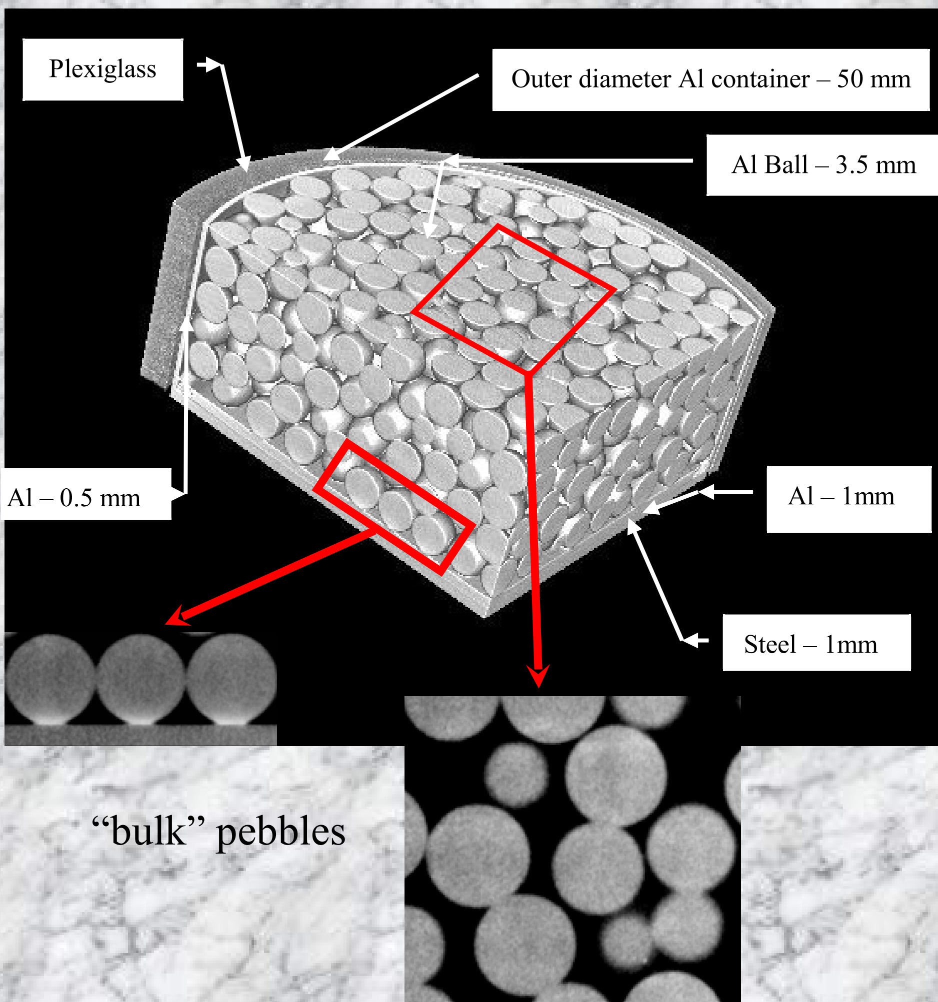

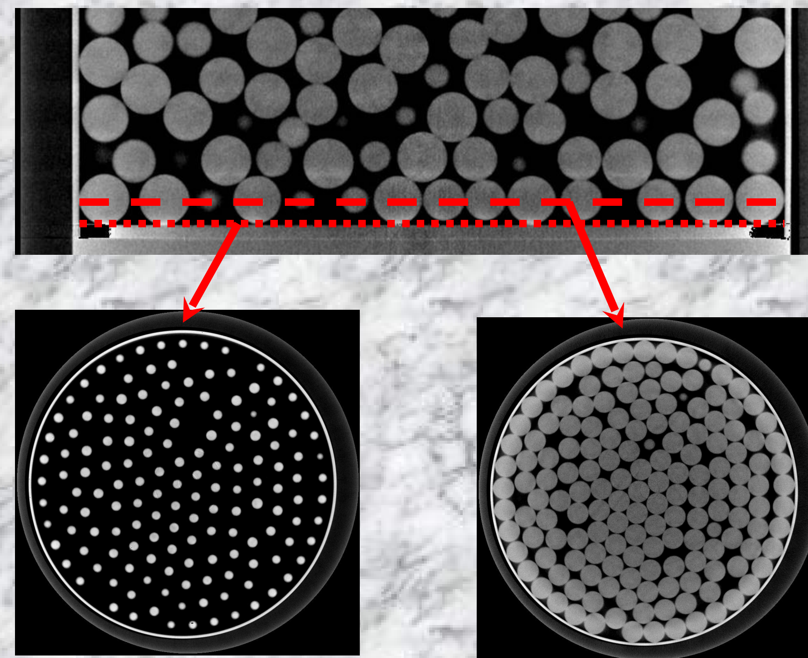

Frontal cross-section (top) axial cross-sections through contact area between steel plate and aluminum pebbles (bottom-left) and through middle of bottom layer of aluminum pebbles (bottom-right)

CFC-JET/ITER - Tomography

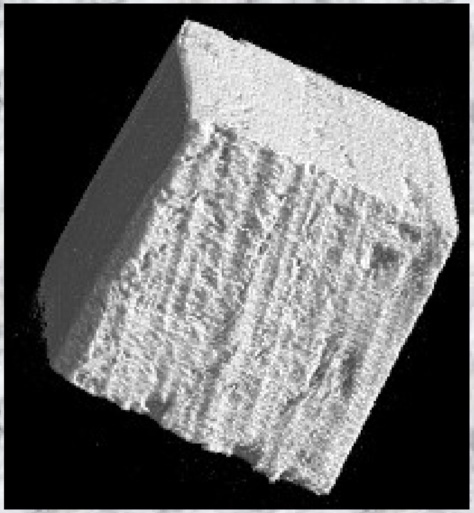

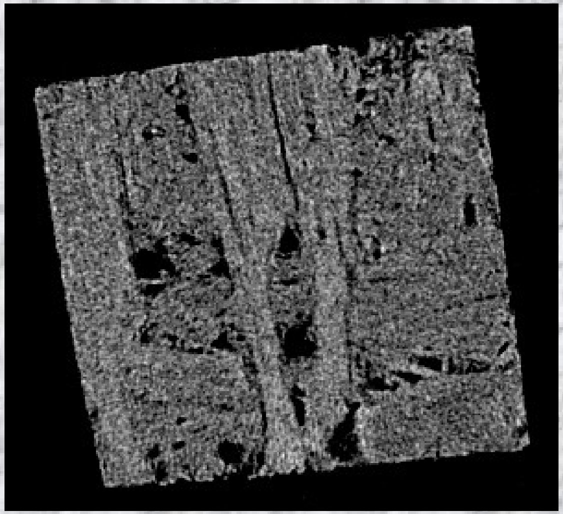

Graphite

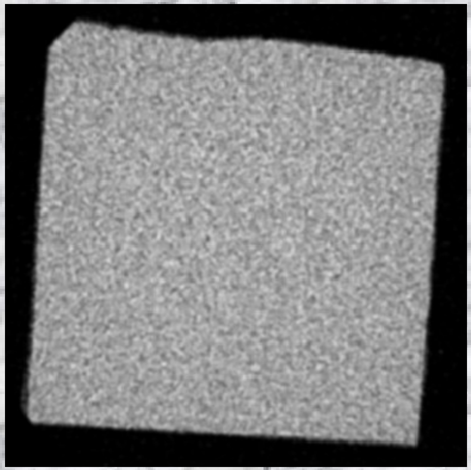

Sample sectioned to about 4 x4x4 mm^3: 3D tomography reconstruction and axial cross section
Space resolution 18 microns/ image pixel, minimum detectable feature 15-20 microns

ITER- Welded Steel Pipe with Cu cables

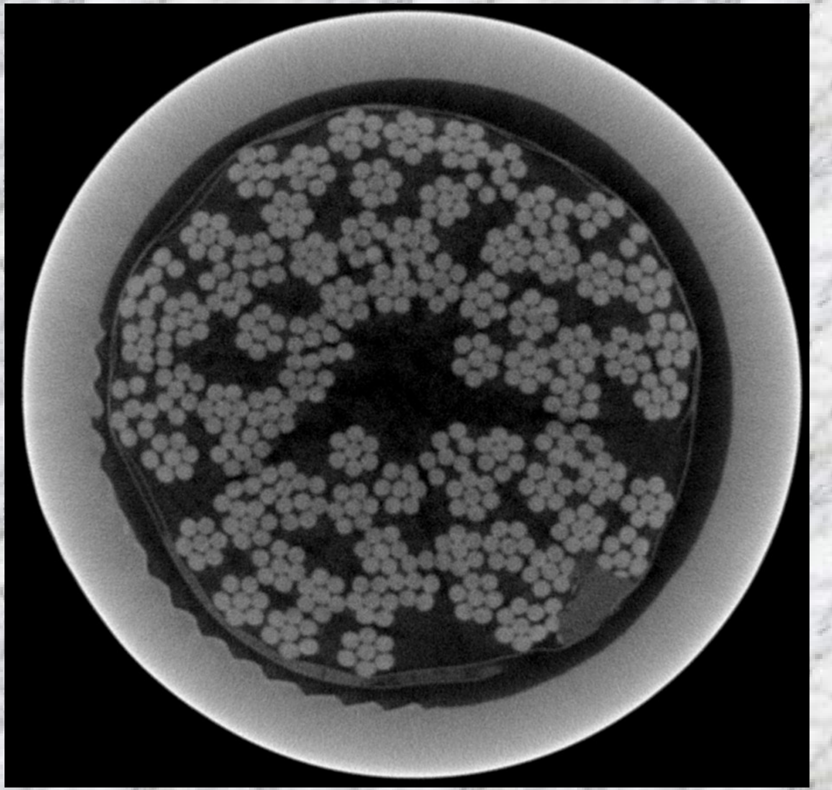

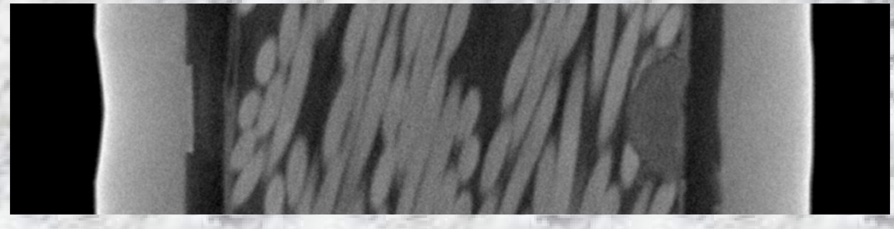

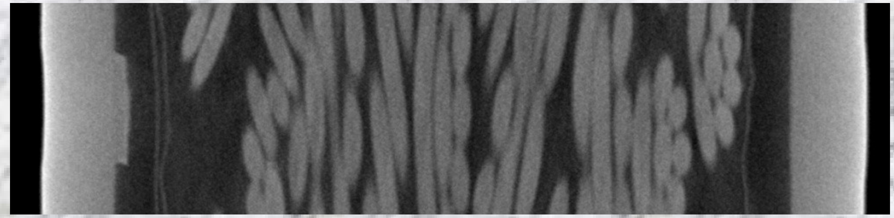

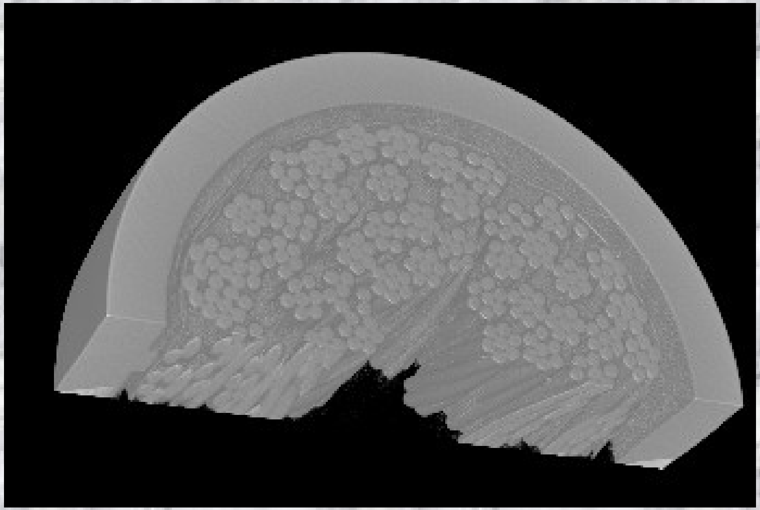

Microtomography measurements with 17 microns space resolution

Welding steel pipes: offset position of the pipes

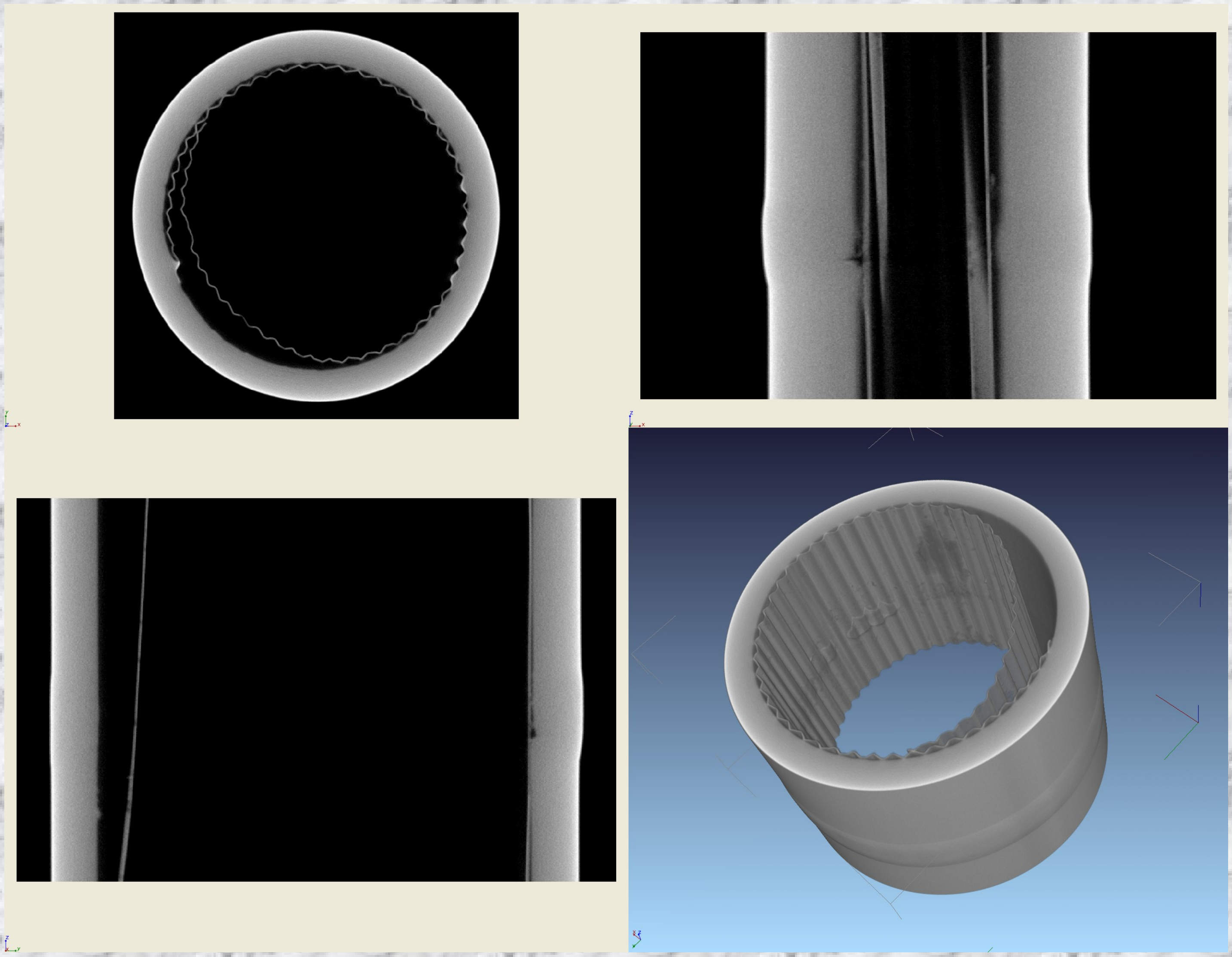

3D X-ray micro-tomography

3D X-ray micro-tomography (μCT) for to the characterization of structural integrity of Nb_3Sn superconducting wires of differing topology

- Detection of the manufacturing defects and anomalies inside the complex structure
- Filamentary Twist Pitch factor evaluation

The evolution of the density distribution of ceramic samples manufactured by Field Assisted Sintering Techniques (FAST)

- sinterized Ni powder and high density MgB_2 superconductors

X-ray microtomography on ITER Type Nb3Sn superconductor wires

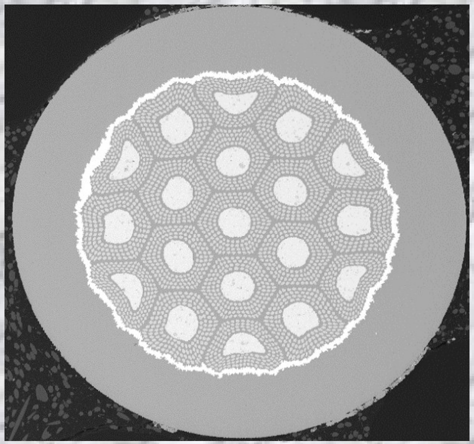

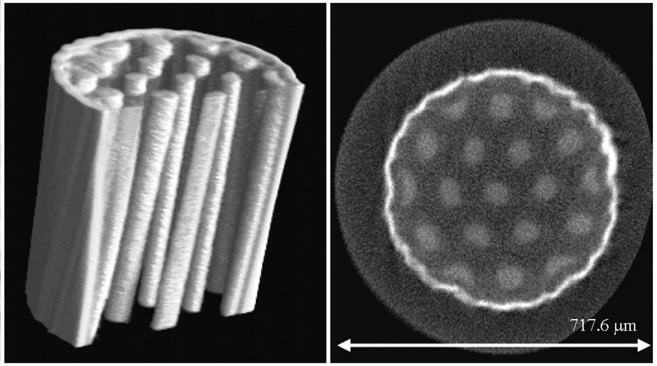

Oxford Instruments (OST), for ITER Type I
0.81 mm (NbTi)3Sn strand, 19 subelements), Single Ta barrier, Cu:non-Cu ratio 1

OST strand of 0.7 mm Nb3Sn filaments

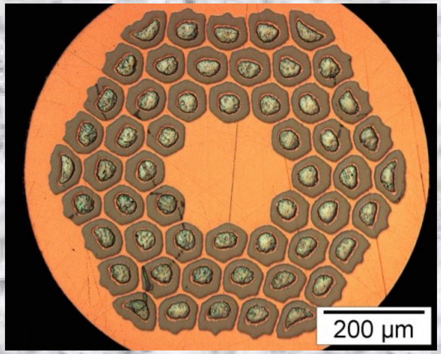

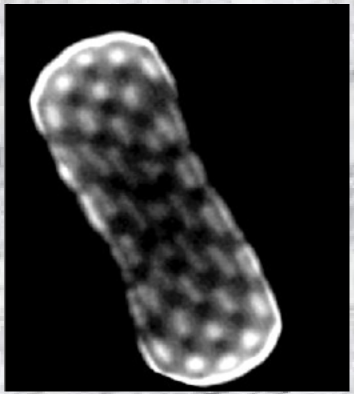

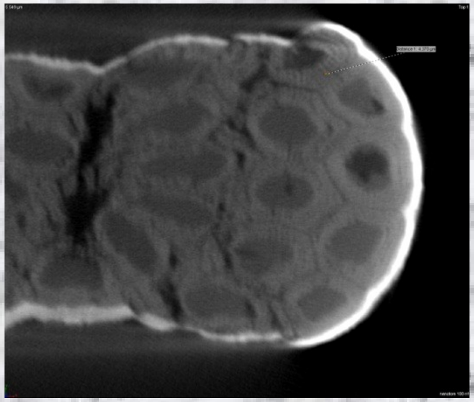

Voxel resolution (from left to right): 3 µm, 1.7 µm & 0.8 µm

Innovative method for non-invasive twist-pitch measurement

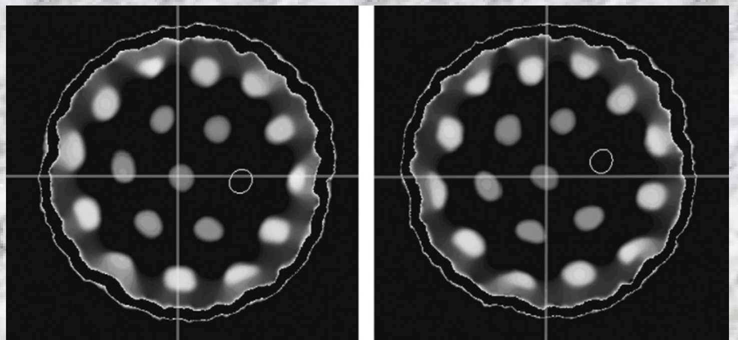

Filaments evolution inside the cross-sections, revealed after filtering and segmentation.

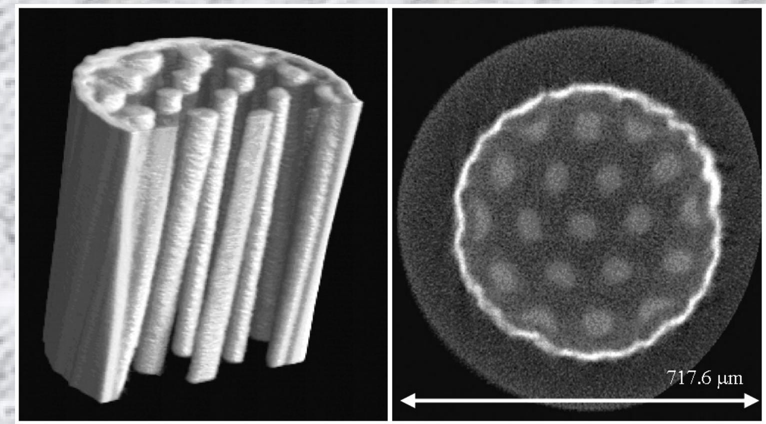

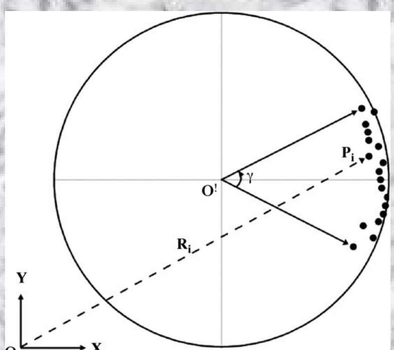

Illustration of the method for twist-pitch calculation

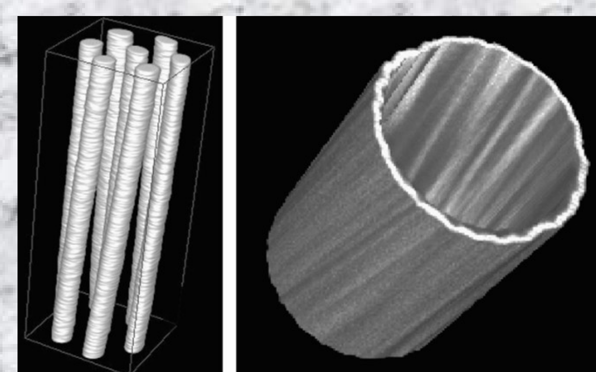

Extraction of the central filaments (left) and of the Ta sleeve (right).

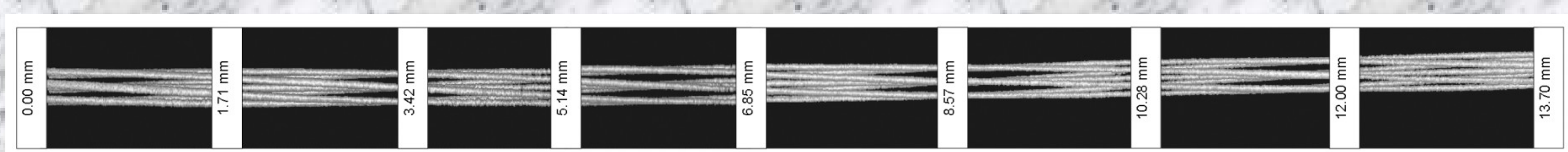

The evolution of twisted structure revealed by screwing together successive tomographic reconstructions TP=15.2 ± 4% mm

Traditional vs. non-invasive methods for measuring the filamentary twist pitch (TP) parameter

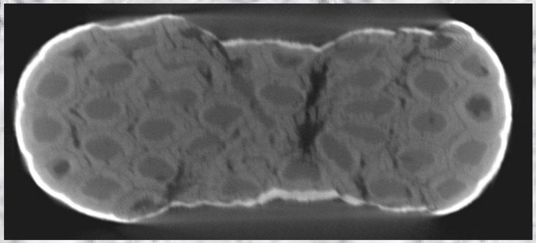

The traditional method for measuring the filamentary twist pitch (TP) parameter consists of a 0.5 mm lamination followed by etching the copper in a nitric acid solution, thus evidencing the twisted structure despite of the Ta barrier.

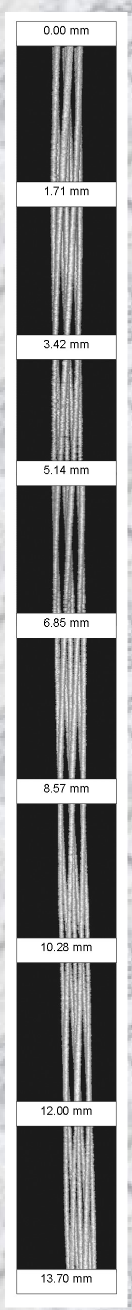

<u>Results</u>
TP=14.7 ± 1 mm (traditional)
TP=15.2 ±4% mm (non-invasive)
Manufacturer specifications 15 mm

Voids formation in MgB2 superconducting wires

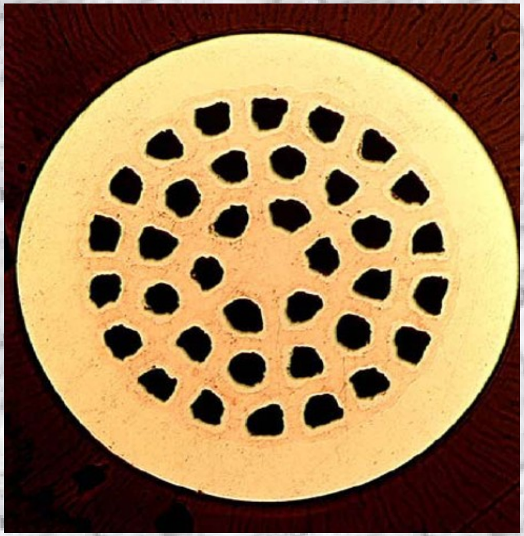

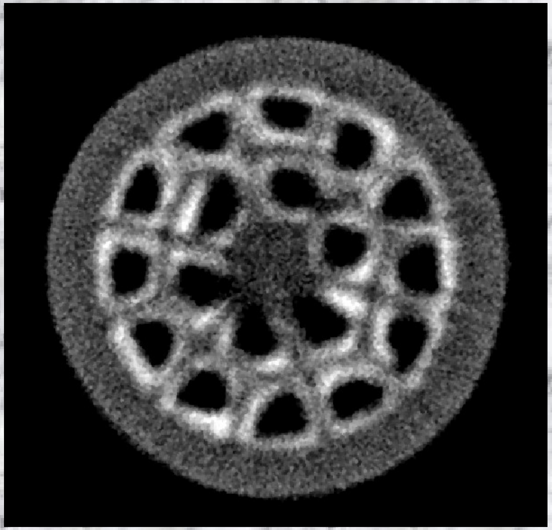

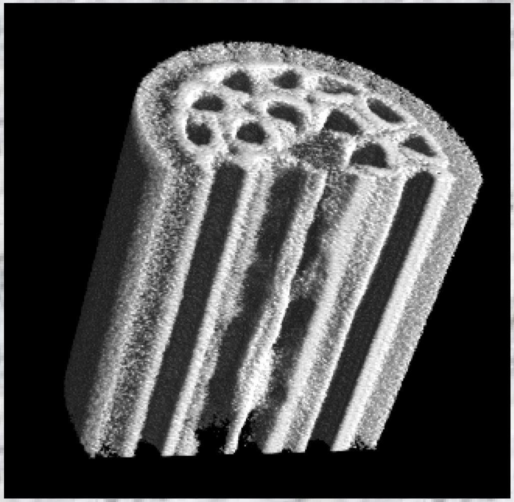

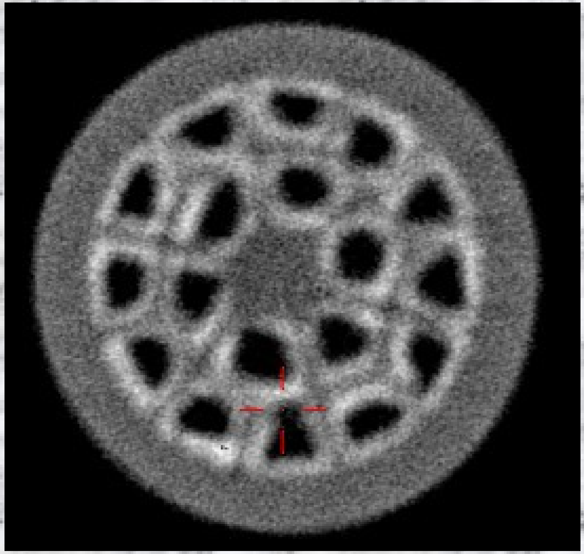

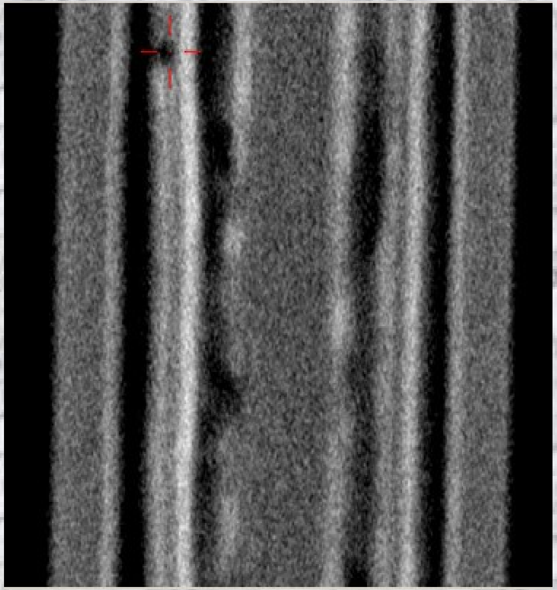

Structure and morphology of high density MgB2 superconductor

- High density superconducting MgB2 (undoped and doped with SiC and B4C) is prepared using FAST (Field Assisted Sintering Technique) from very porous and mechanically weak mixture of Mg and B.

- Although, at present, it is not possible to significantly advance the understanding of the milling-properties relationship, μCT can reveal clear differences between the samples.

- For our particular bulk MgB2 superconducting samples, μCT allowed observation of certain 3D density patterns and their evolution with the milling time of the precursor mixtures.

- We shall emphasize that one important limitation of the μCT is that it cannot give any information on crystal quality and composition.

MgB2 samples and processing conditions

Sample	Mixing/milling	Heat treatment temp. (°C)	Heat treatment time (h)
A	Manual in Ar	700	1h
B	Mechanical milling in Ar, 0.5h	700	1h
C, C1	Mechanical milling in Ar, 1h	700	1h
D, D1	Mechanical milling in Ar, 3h	700	1h
E	Mechanical milling in H_2, 0.5h	700	1h
F	Mechanical milling in H_2, 1h	700	1h
G	Mechanical milling in H_2, 3h	700	1h

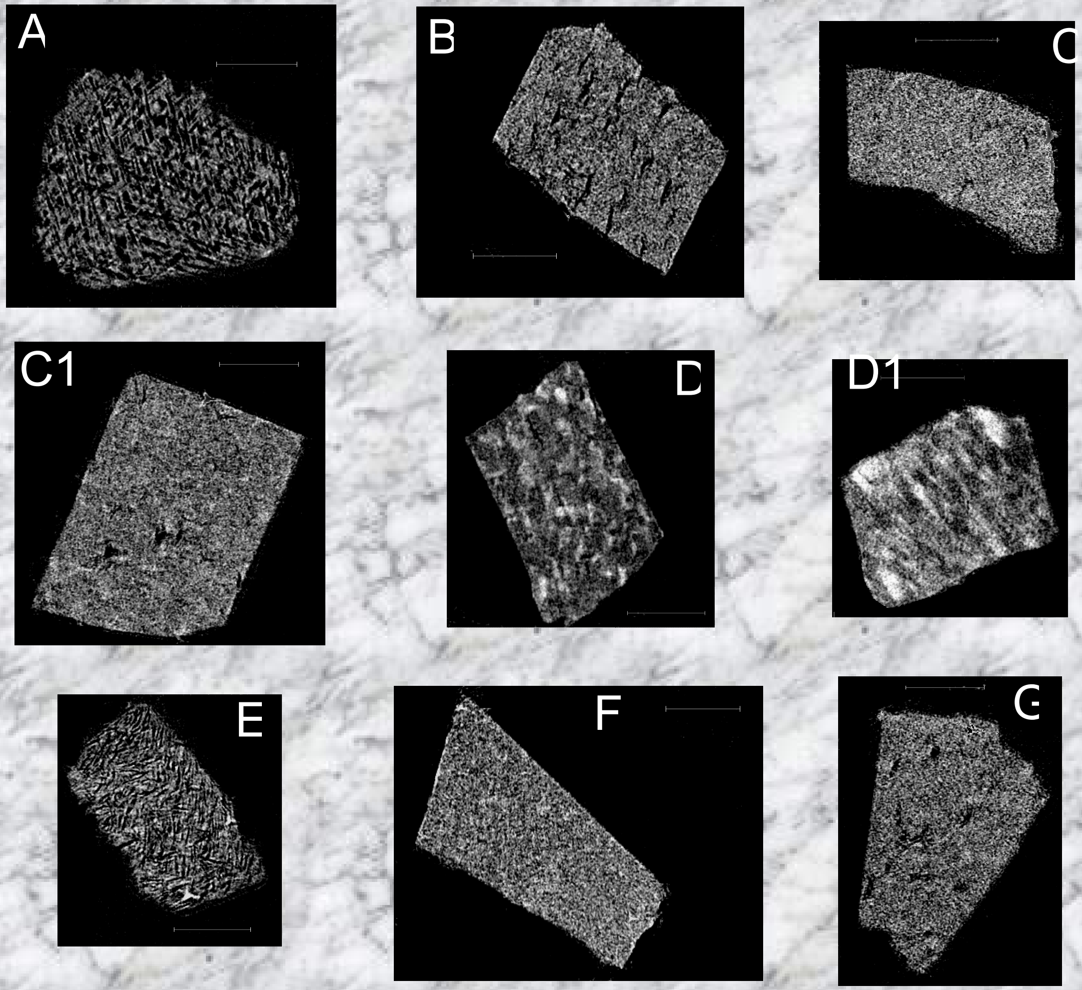

Representative µCT images of the heat treated bulk samples. Images were taken for a voltage of 40KV and a current of 100µA, sampling rate 3.87µm.
Scale bar is 100µm.

Summary

X-ray micro-tomography may represent an appropriate solution for the microstructural investigation of relevant material issues as identified during manufacturing processes in a number of cases when the traditional techniques are not sensitive enough or are not the most appropriate to reveal the key characteristics of the investigated advanced materials.

Neutron emission tomography for limited data set at JET tokamak

KN3 tomography

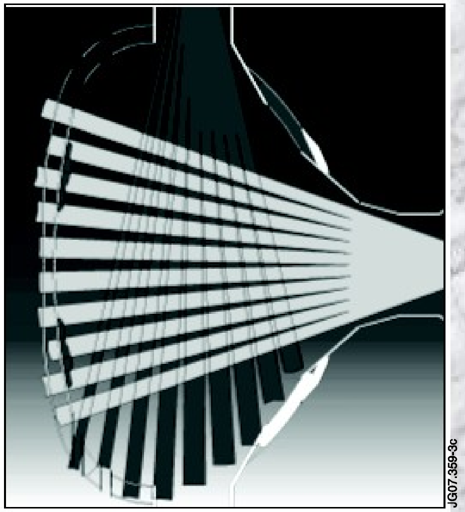

Highly undetermined problem:

- 19 equations
- 35 X 20 unknown

(90 mm pixel size)

Maximum likelihood solution

The emission is assumed to be a Poisson process, and **P_{km}** is a sample from a Poisson distribution whose expected value is:

$$\sum_i w_{ik} f_i$$

Then, the probability of obtaining the measurement **p** if the image is **f** is the so-called **likelihood function:**

$$L(P/F) = \prod_k \left[\frac{1}{p_k!} \left(\sum_i w_{ik} f_i \right)^{p_k} \times \exp\left(- \sum_i w_{ik} f_i \right) \right]$$

Smoothing

Smoothing in magnetic surfaces may supply the lack of information.

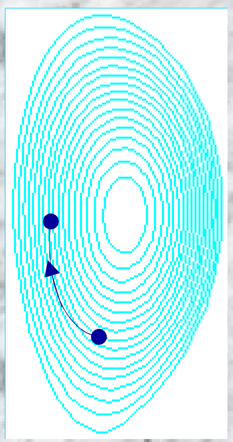

$$f_i = \sum_{\substack{j=-w_{med} \\ w_{med} \in L_k}}^{j=+w_{med}} m_{ji} h_j$$

median filtering using a circulating window along the magnetic contour lines

Additional smoothing can be obtained by resampling the experimental projection. Projection resampling implies the introducing of virtual lines of sight which ensures an improved coverage of the reconstruction domain

Testing the method - phantoms

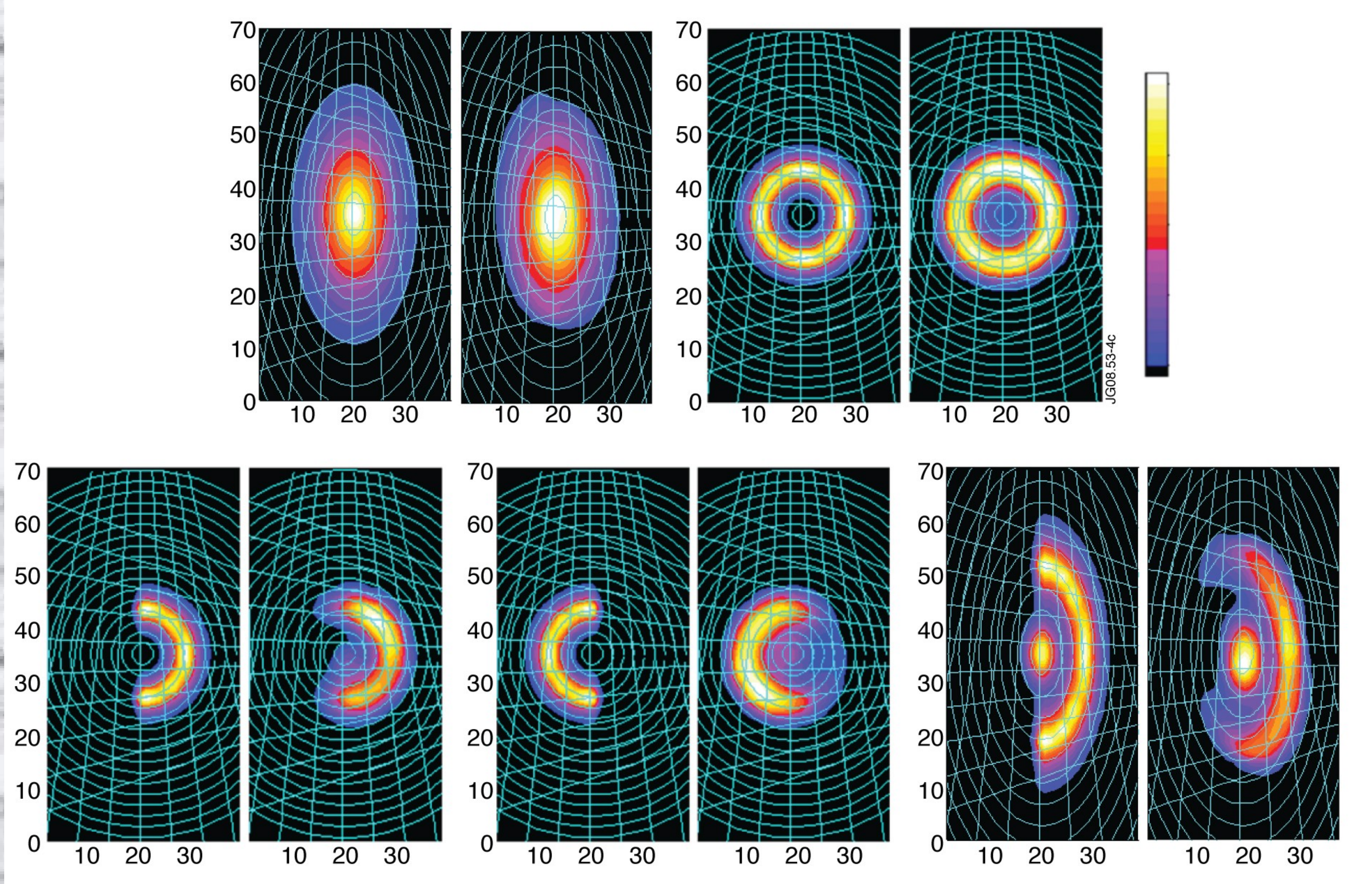

Information about the temporal evolution of the neutron emissivity

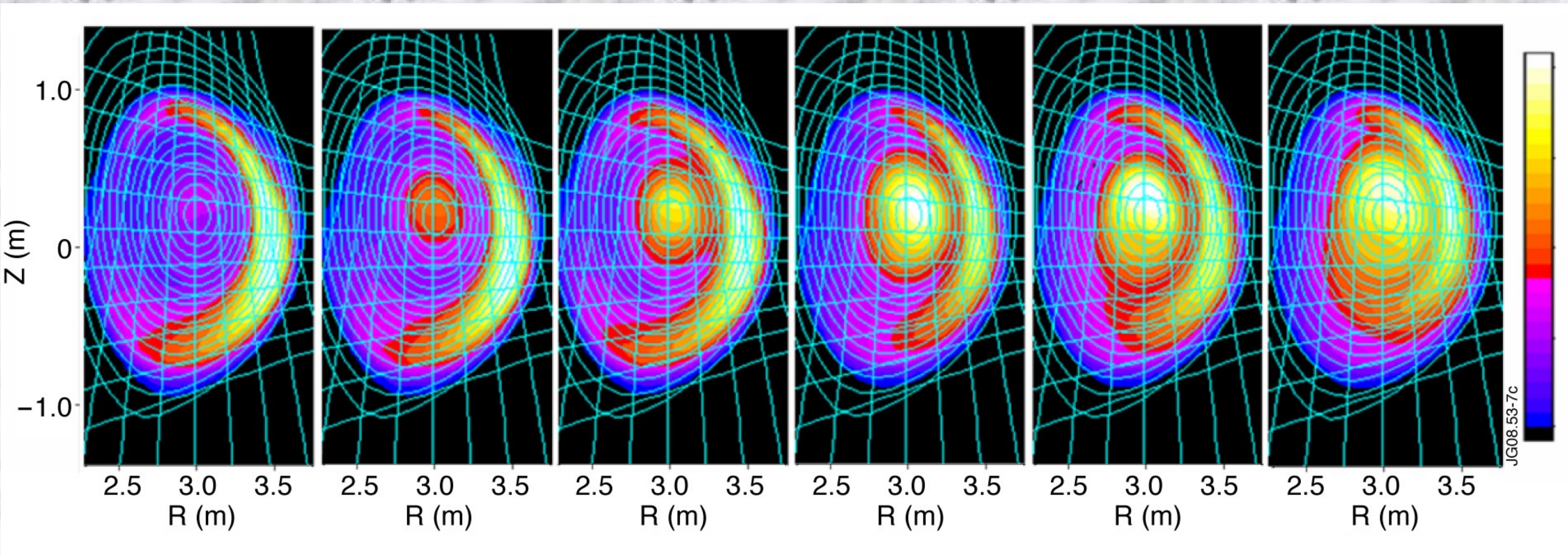

Temporal evolution of the D-T 14 MeV neutron emissivity in a trace tritium experiment showing the relaxation of the high density plasma, which is heated by D neutral beams after the T-puff - shot 61141 (from 60.87 s to 61.32 s).

Nuclear waste management:
Combined 3D tomography and X-ray fluorescence for host rock

Main goal of research was to implement methods for correlation of the host rock structure and composition

- structure determined by X-ray tomography
- composition determined by X-Ray fluorescence
- structure & composition determined by Dual Energy Tomography
- Fabrication of a microbeam fluorescence facility for surface composition mapping (20 μ resolution)
- Implementation of innovative combined transmission-fluorescence tomography method

X-ray tomography measurements on Grimsel sample

- 2D CT for full sample diameter FOV
- 3D µCT for small sample

2D CT cross section:

high penetration, low space resolution

Scanning parameters:

Linear array 1024 pixels x 0.4 mm pitch
Scanning method translate-rotate
U= 300 kV, I=2.0 mA
1.5 mm Brass pre-filter
Reconstruction matrix: 500x500
Voxel size: 0.25x0.25x0.8 mm^3

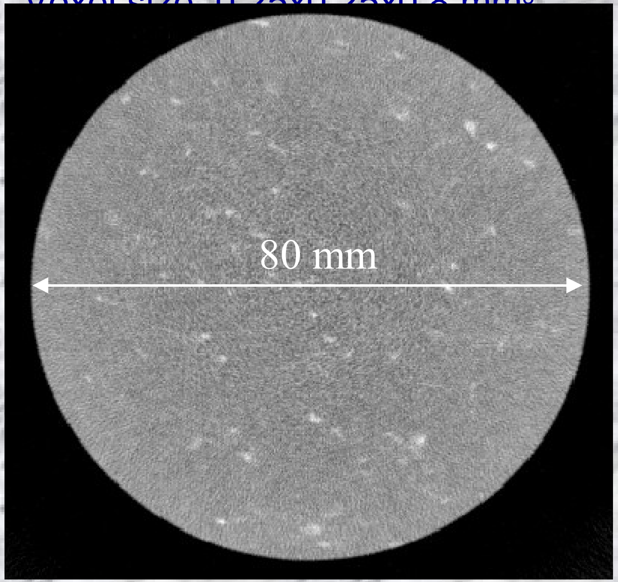

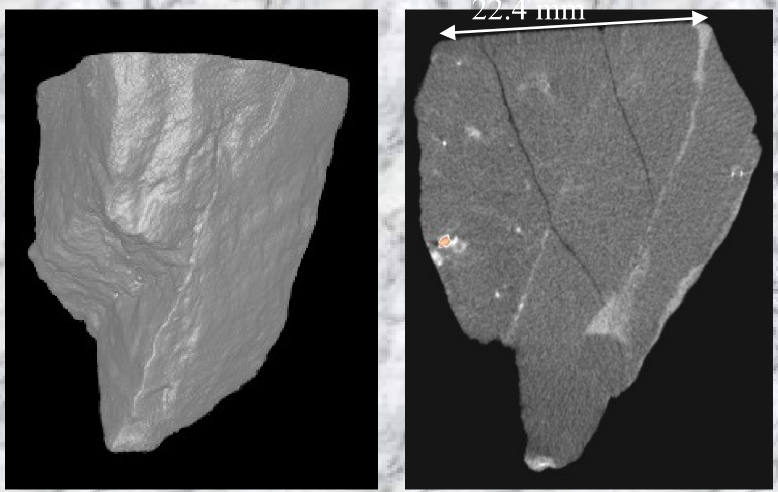

3D µCT and axial cross section

Scanning parameters:

Flat panel array 1220x1216 pixels x 0.1 mm pitch
scanning method rotate-rotate
U= 100 kV, I=0.08 mA
Cd & Cu pre-filter
Voxel size: 46x46x46 μ^3

Fully 3D macro CT : high penetration, low space resolution

Scanning parameters:

Source Bosello 450 kV , focus size 0.3 mm
U = 370 kV, I=1.5 mA, 720 projections full scan, Prefilter Brass 2 mm,
Detector PE 1640 AN1 ES CT – 1024x1024 pix2, 16 bits, 0.4x0.4 mm2
Source – Object distance : 519.75 mm
Source – Detector distance : 1505.3 mm
Magnificattion 2.9
Voxel size 0.138x0.138x0.138 mm3

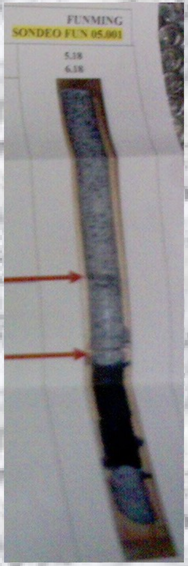

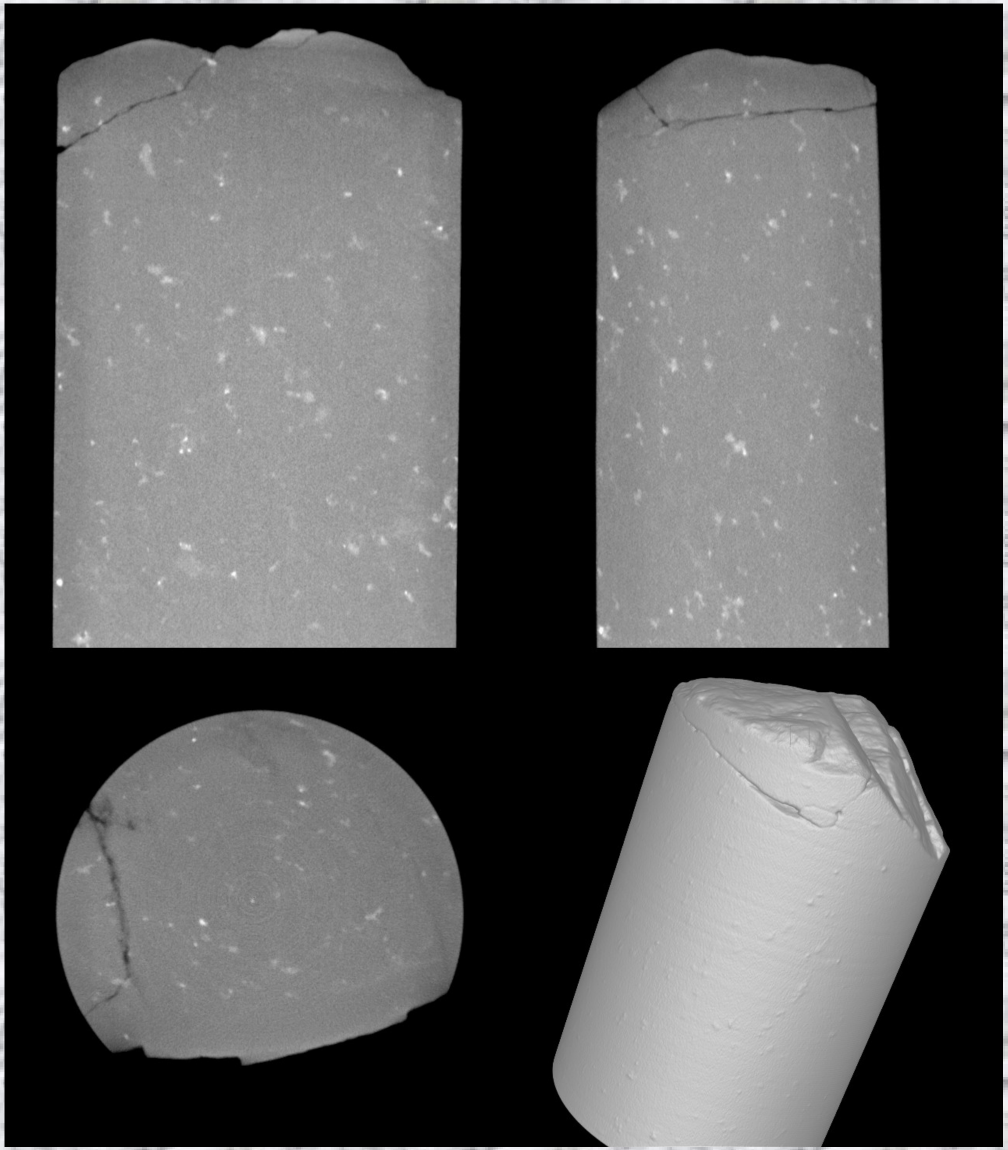

METHODICS DEVELOPMENT

- Micro-cavities extraction procedure

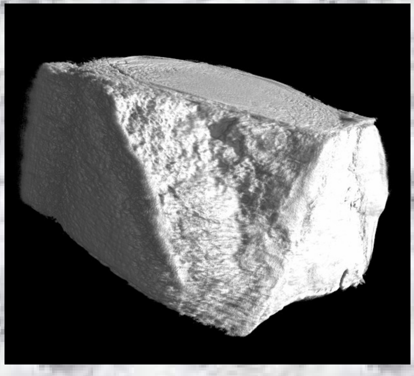

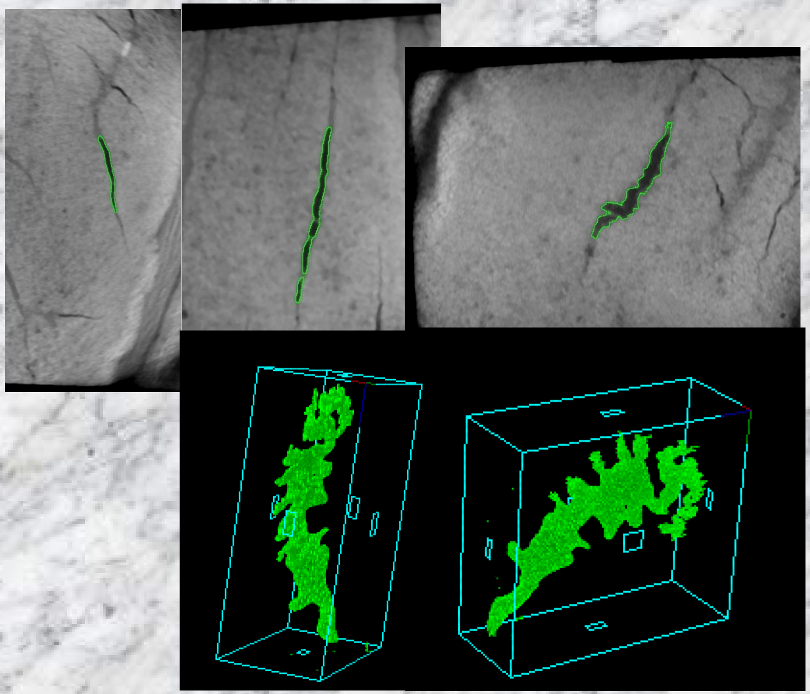

Tomography reconstruction of a crystalline rock axial, frontal and sagital cross-section. The region of interest is marked in green and the cavity is extracted by a sequence of image processing algorithms that finally provides the 3D cavity boundaries.

High-Resolution Cone Beam Tomography for Two-Phase Flow Diagnostics

Cone-Beam CT for two-phase flow

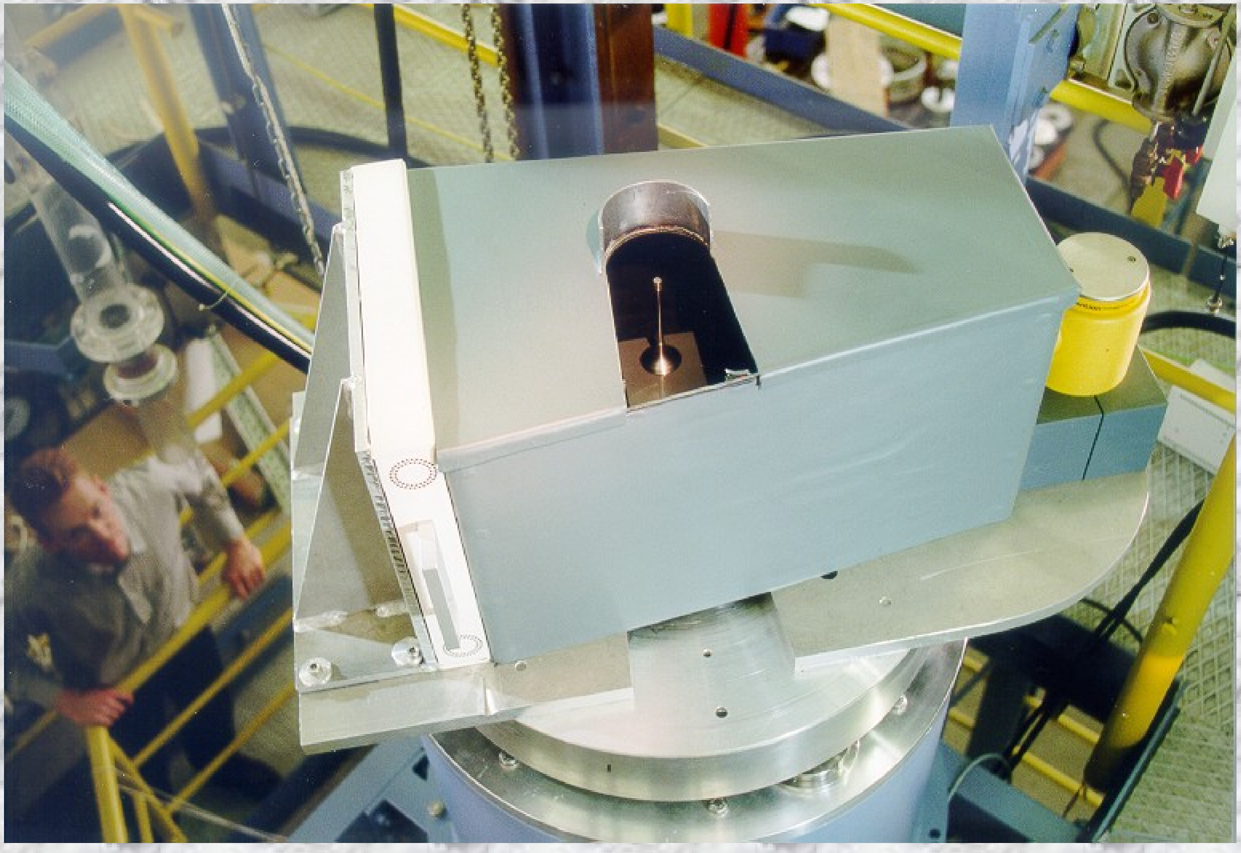

Upward bubbly flow
7 nozzle injection β=3.25%, jl=1.8 m/s, Height = 40D

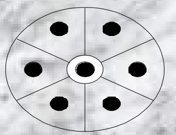

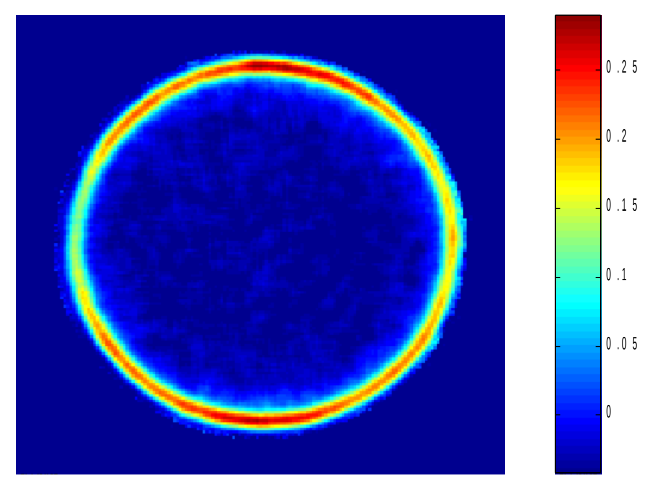

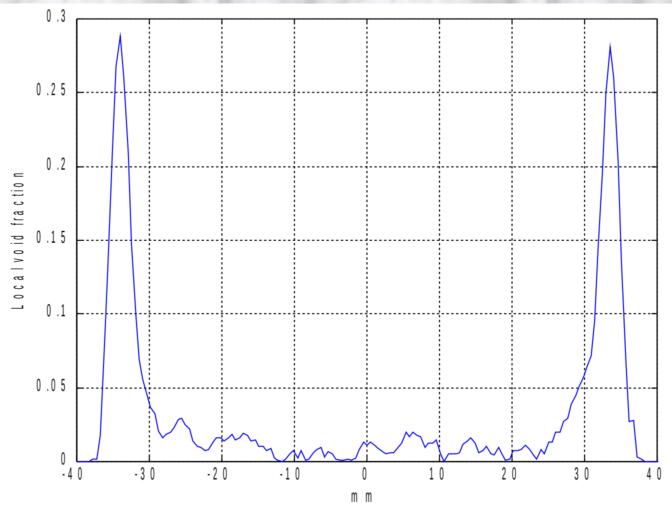

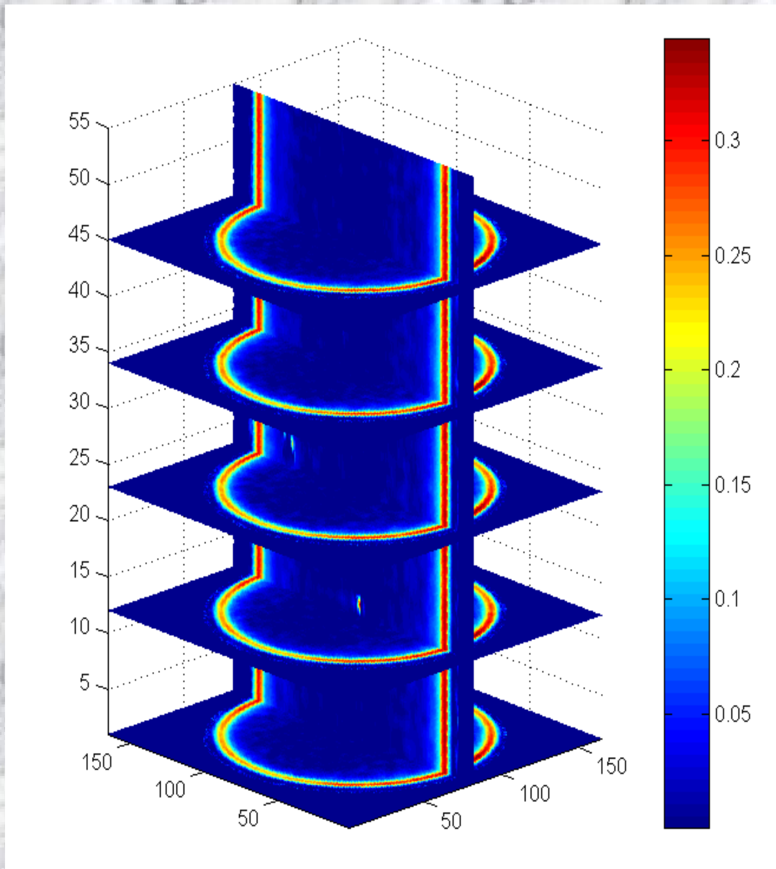

Ultra fast X-Ray Computed Tomography for Transient Phenomena

Specifications

Number of sources	18
Scanning time	3.8ms
Scan rate	258 slices/s
Number of detectors	256 pixels
Detector pitch	1.425mm
Max. object diameter	50mm I.D.
Image reconstruction	Filtered back projection

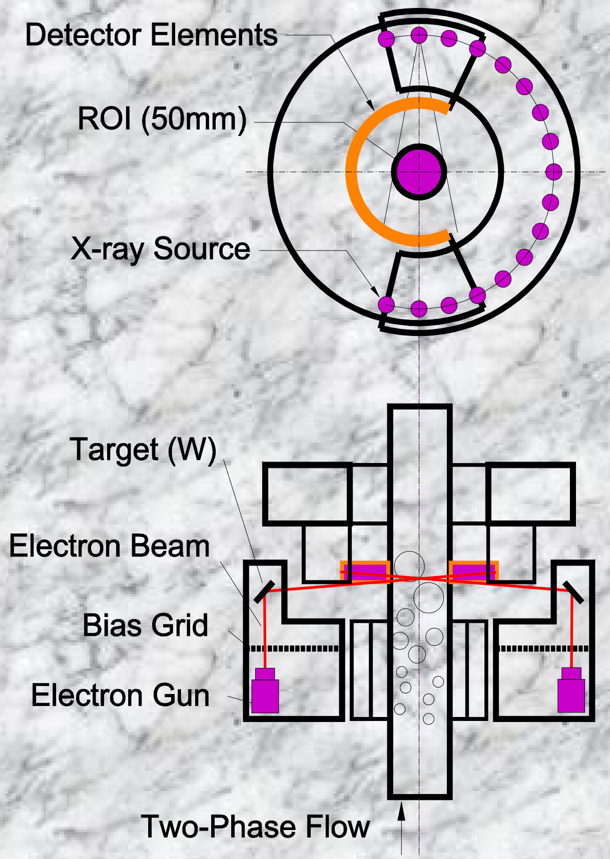

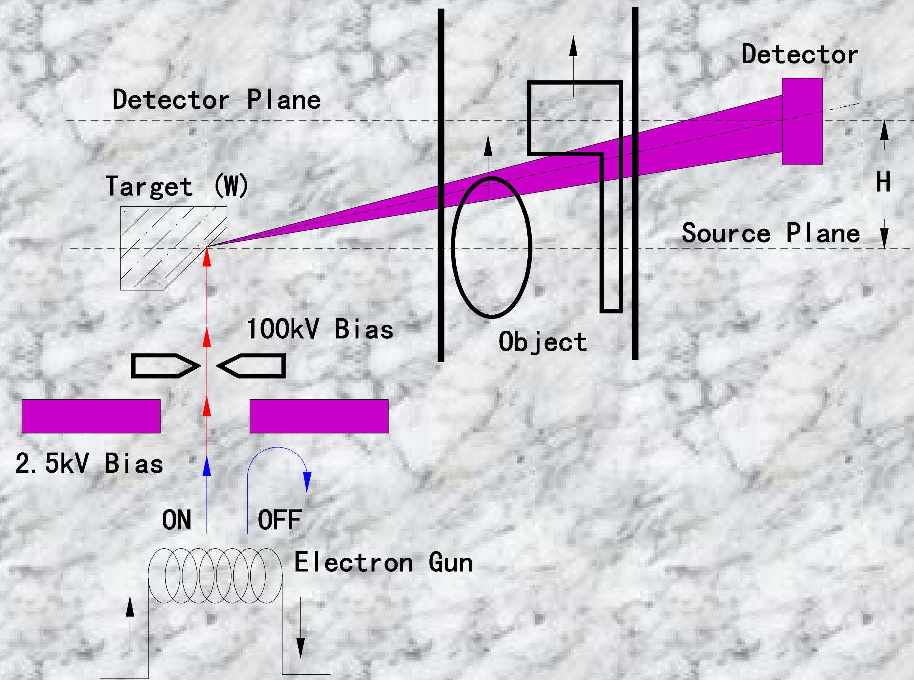

Construction of Fast X-ray CT

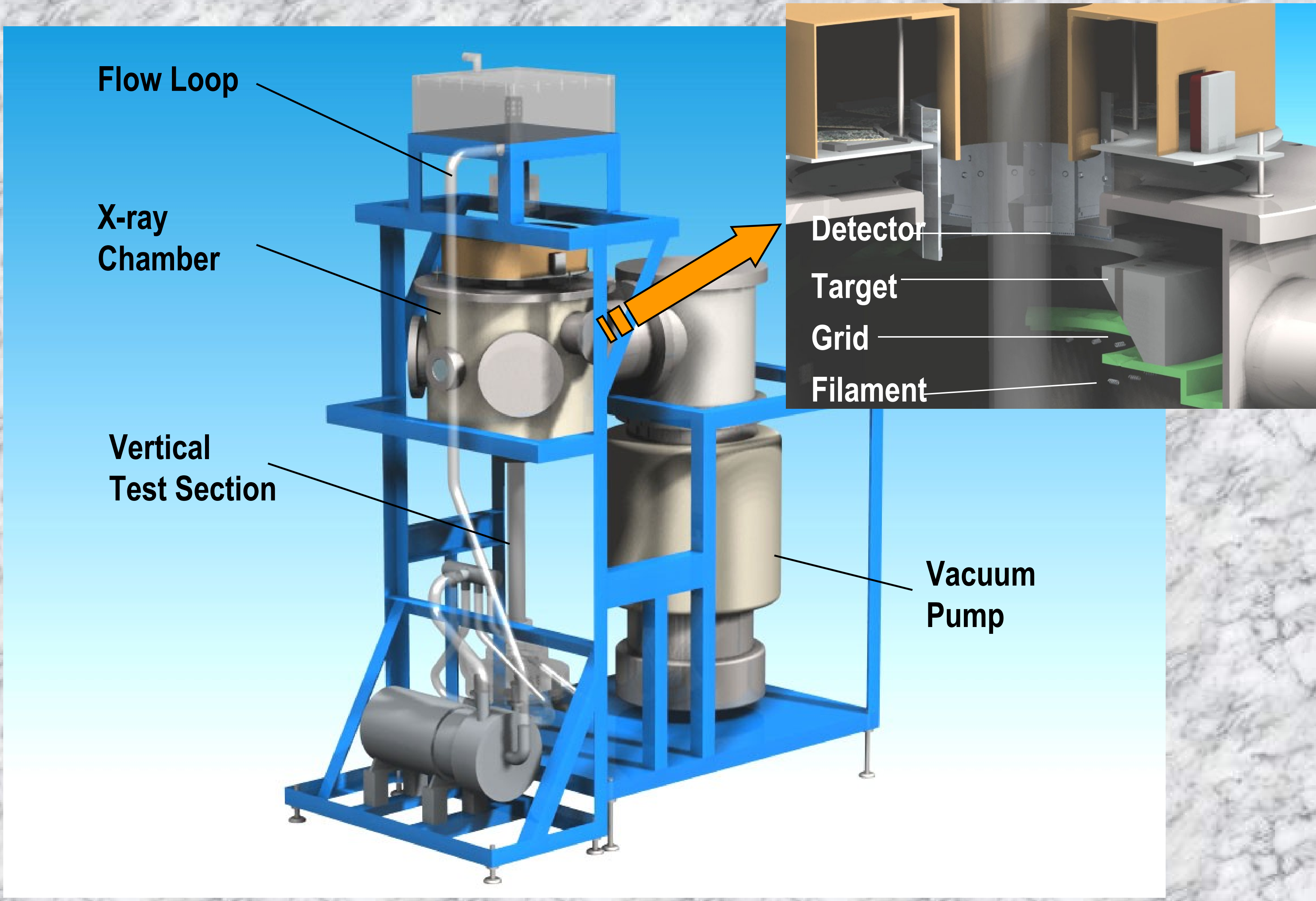

Instantaneous Bubble Interface Visualized by Fast X-ray CT

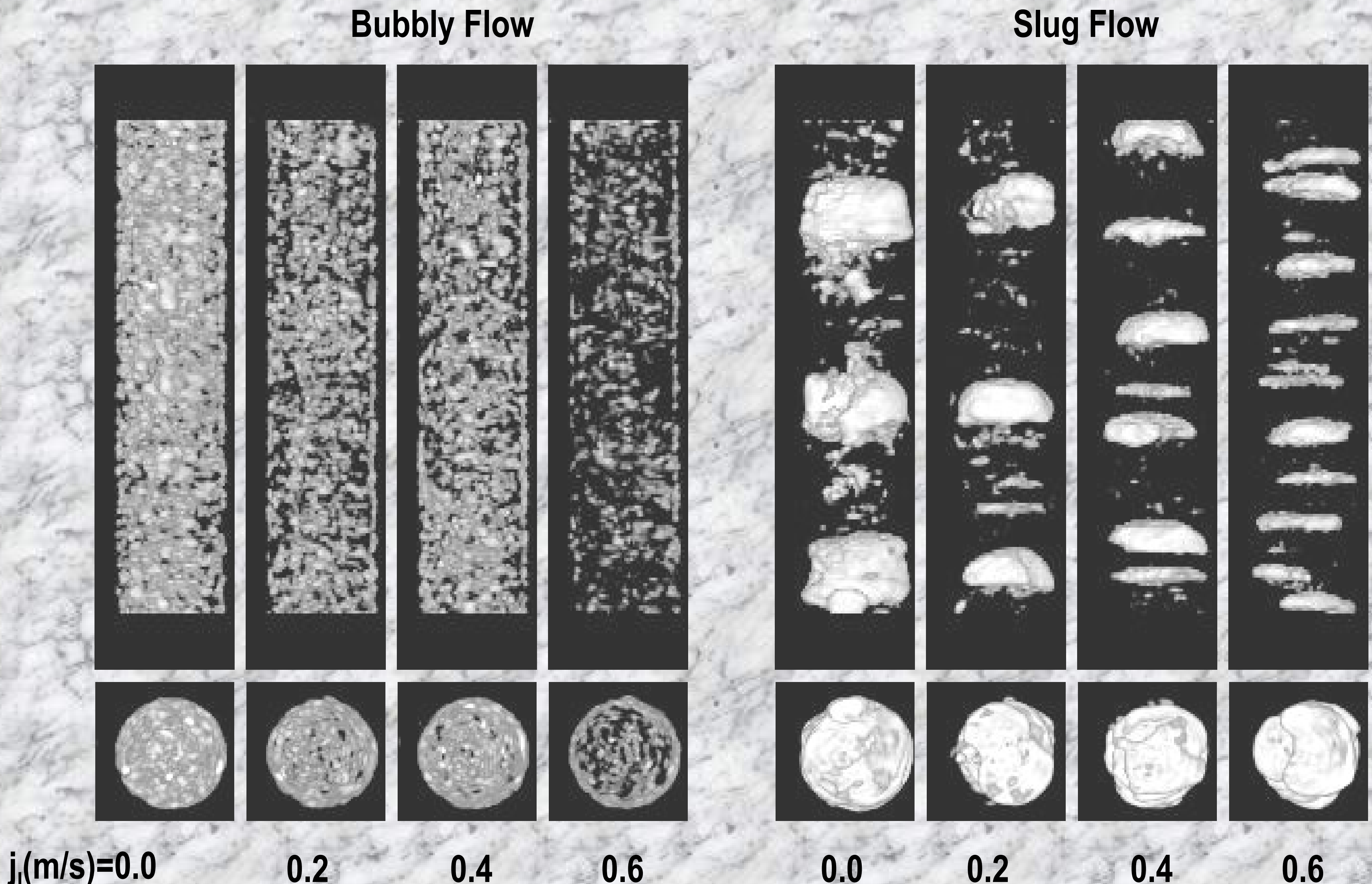

(1.0sec.,
j =0.15m/s)

Void Fraction and Integrated Bubble Perimeter in Flow Channel Cross Section

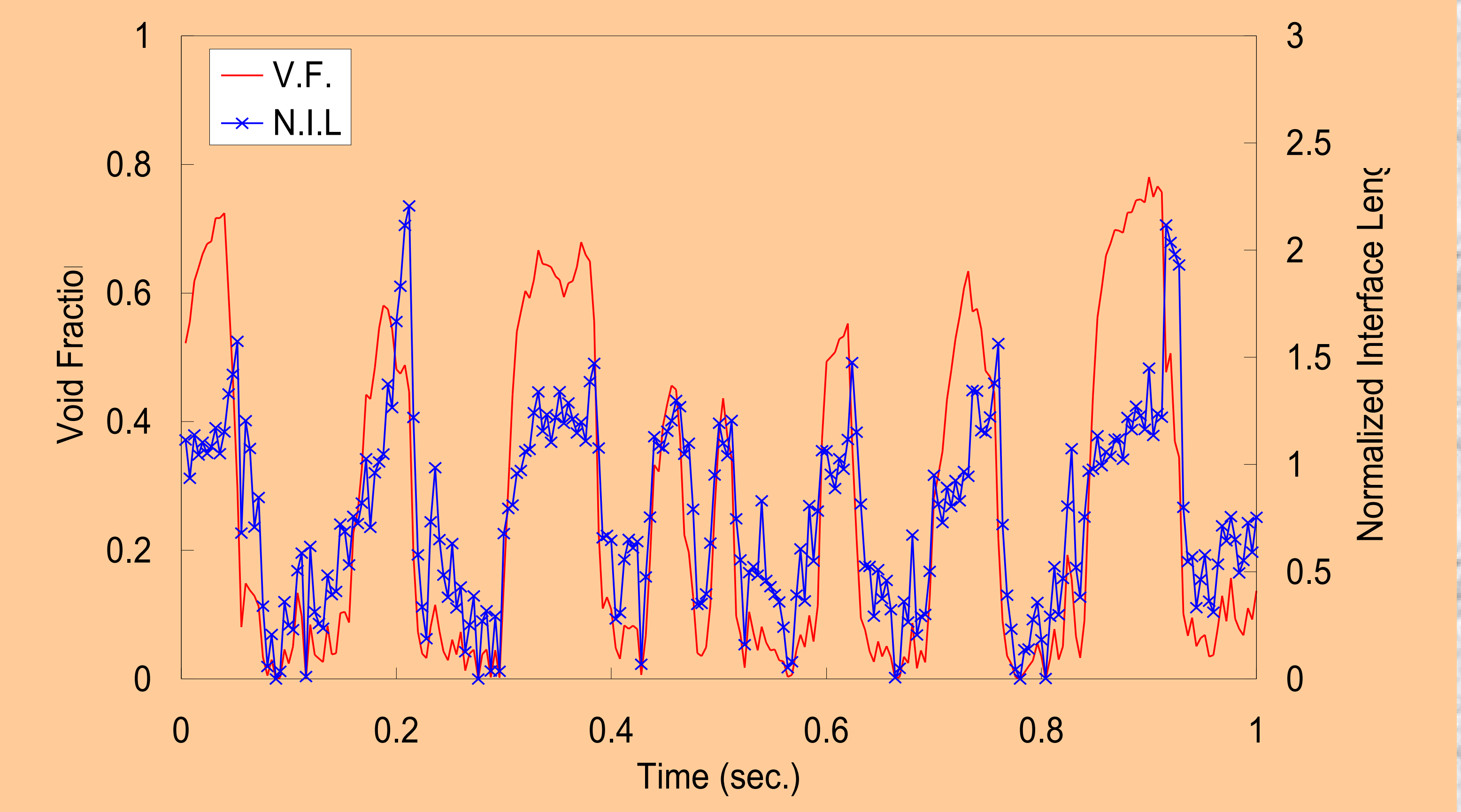

Flow

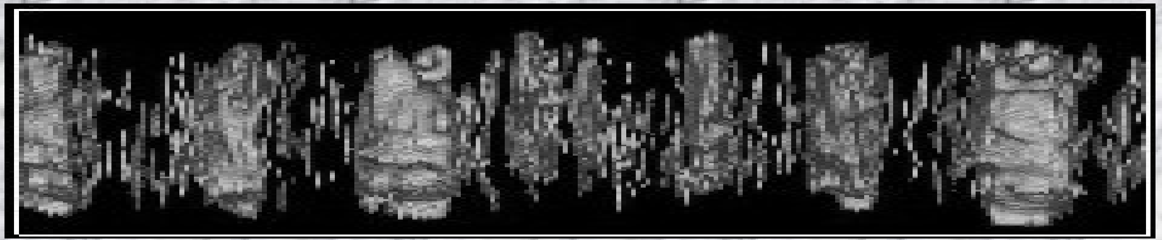

jg=0.385m/s, jl=0.621m/s

Experimental Parameters in Fluidized Bed Test

Fluidized Bed Composition
(from T .Kai with Univ. of Kagoshima)

SiO_2+Al_2O_3	(13% : 87% by weight)
Particle Diameter:	36 mm (average)
Solid-alone density :	2600 kg/m^3
Porous density:	980 kg/m^3
Loosly-packed density:	560 kg/m^3

Fluidized Bed Test Section

Orientation:	vertical
Static height:	860mm
Tube Outer Diameter:	50mm
Tube Inner Diameter:	46mm
CT-Measuring Height:	600mm
jg=0.005 - 0.07m/s	

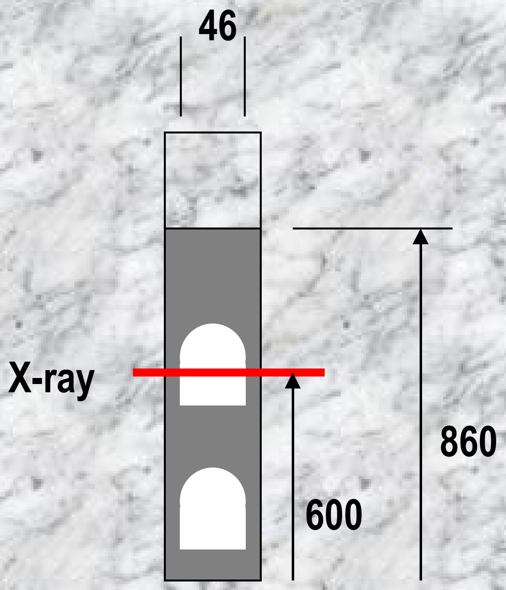

X-ray CT Scanner

X-ray power	100kV, 5mA (Nominal)
Vacuum:	1.2x10^{-6} Torr
ROI elevation	L/D=13.0
Measuring Period	2 sec. (500 slices)

"Bubble" Interface in Alumina Powder

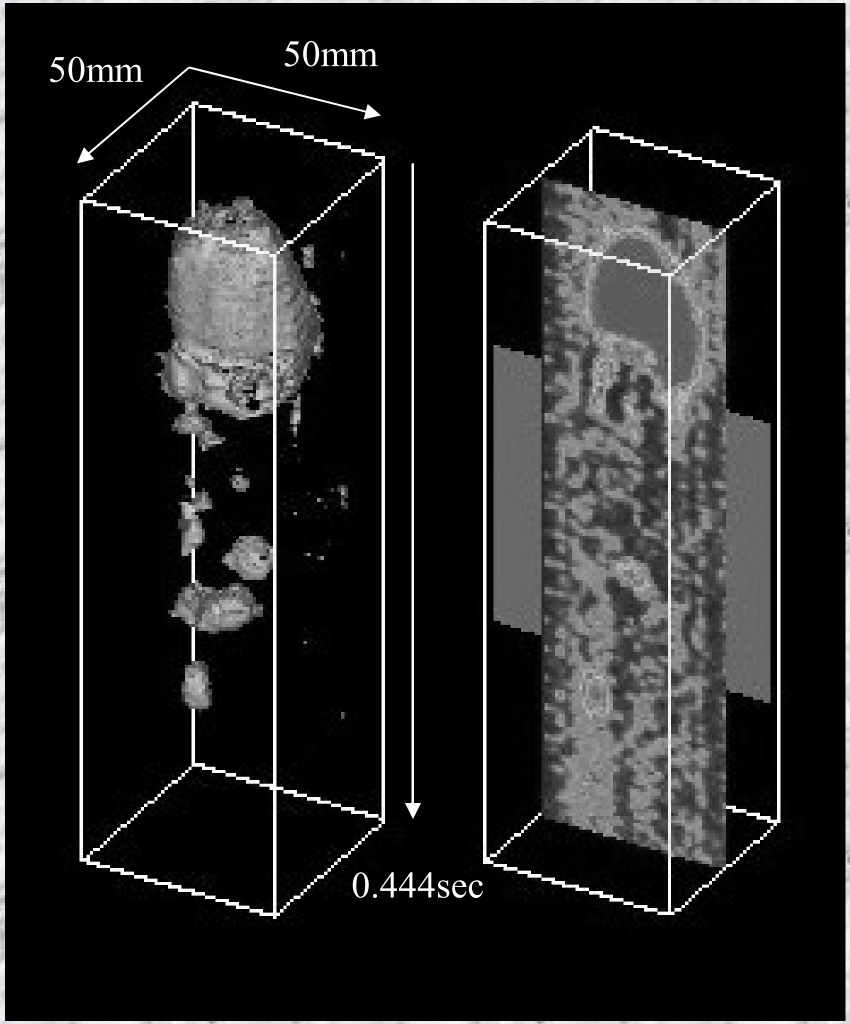

jg=0.04m/s.

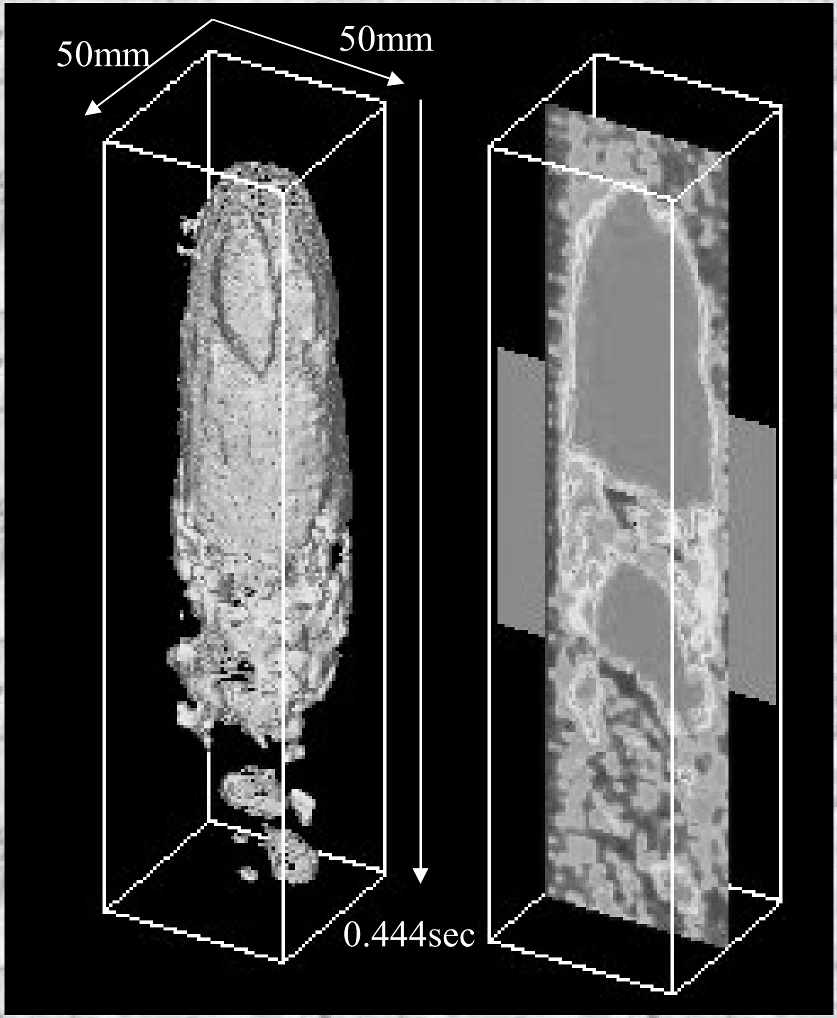

jg=0.07m/s.

Gamma Emission Tomography for Nuclear Fuel Engineering

Principle of Emission Tomography
Maximum Entropy implementation

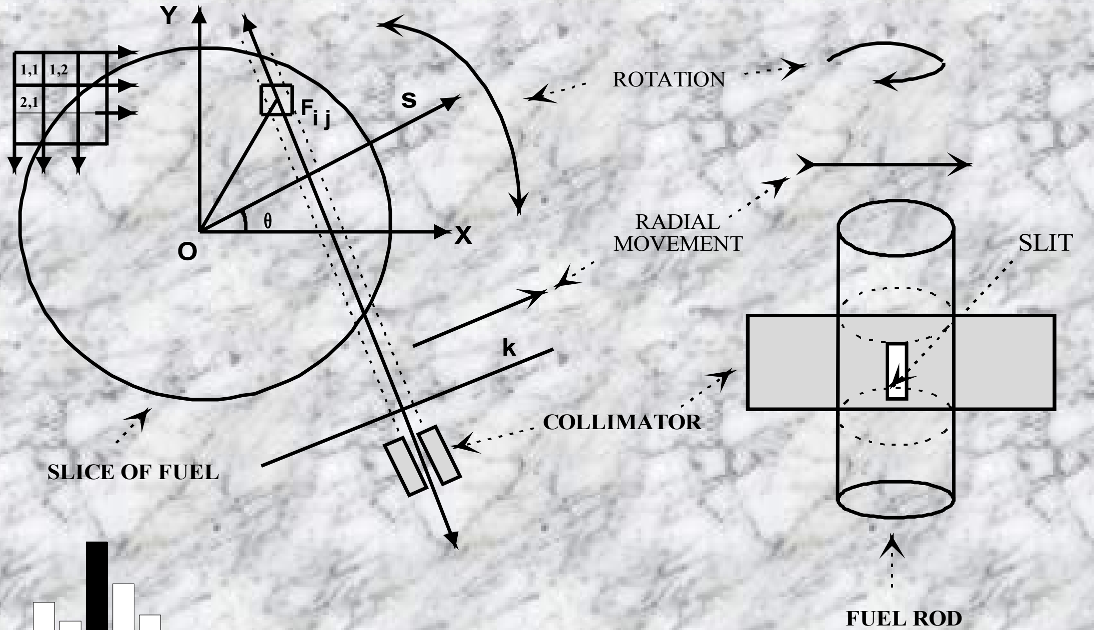

$$p_{km} = \sum_{ij} w_{ij;km} f_{ij}$$

$$w_{ij} = \begin{cases} L_{km} \cap \ \mathrm{pixel}(i,j) \\ \exp\left(\sum_{np} \mu_{np} l_{np;km} \right) \end{cases}$$

$$\Psi = H - \sum_{k=1}^{N} \sum_{m=1}^{M} L(k,m) \cdot \left[p_{km} - \int_{r(m,k)}^{r(m,k+1)} ds \cdot \int_{-\infty}^{\infty} f(s \cdot \cos(\theta_m) - u \cdot \sin(\theta_m), s \cdot \sin(\theta_m) + u \cdot \cos(\theta_m)) du \right]$$

Emission Tomography Equipment

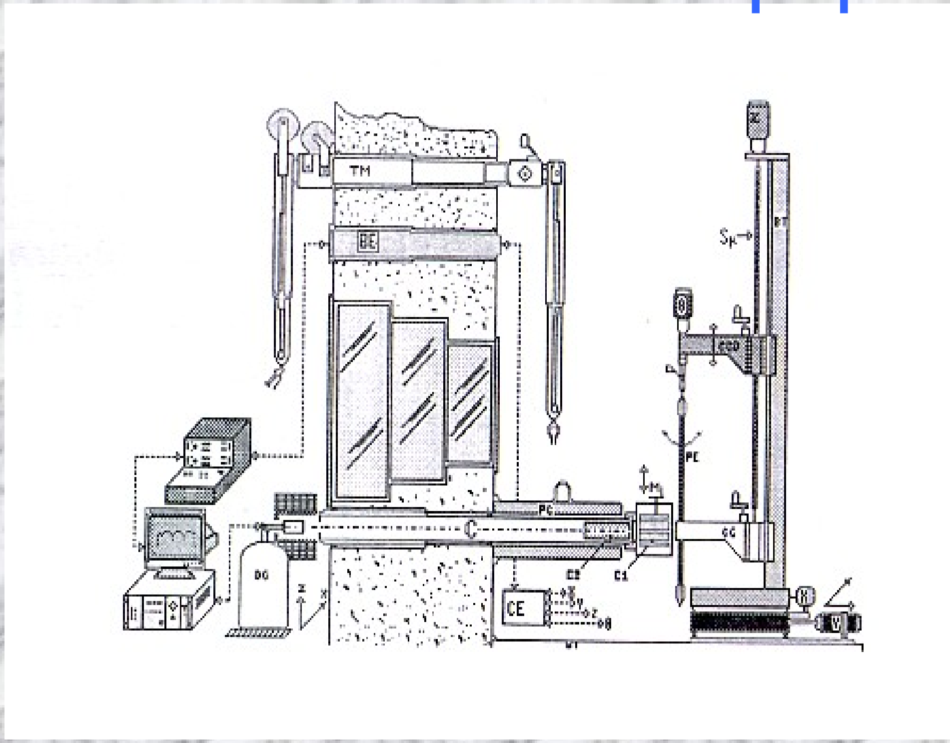

High purity Germanium detector: 18 % Efficiency

Adjustable slit collimator. Height: 5 / 50 mm Width: 0.10/0.25/0.50

Scan device with motion control (ACB). Step motors. Axial/Radial/Rotational.

Multichannel analyzer (ORTEC). Gamma spectra acquisition.

Personal computer. Motion & Acquisition Control. Spectrum analysis. Tomography.

Cs-137 Profile

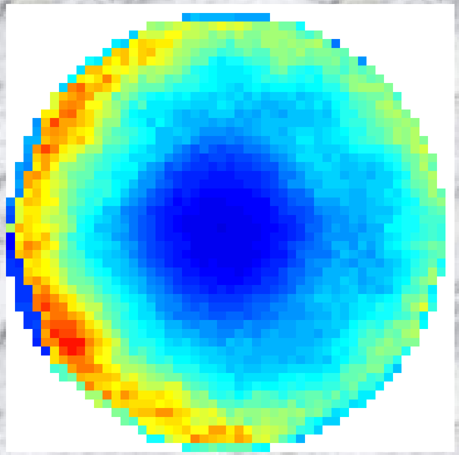

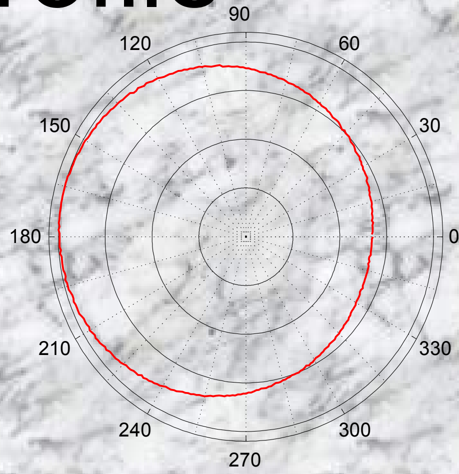

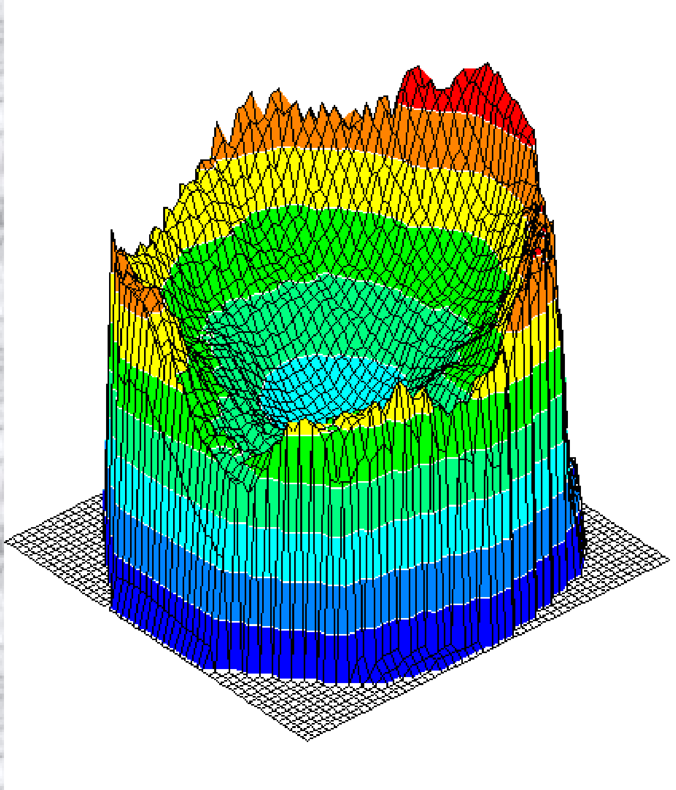

CANDU FUEL - Cs-137 migration

large depression activity in the middle of the rod

- accumulation of Cs-137 in the last mm of the rod
- lack of pellets interfaces

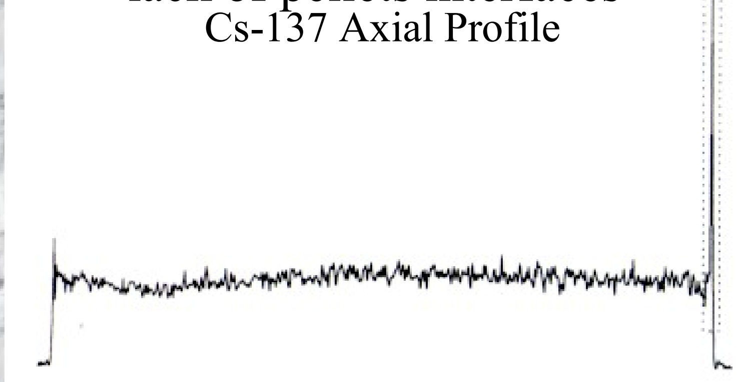

Cs-137 - Intact Rod

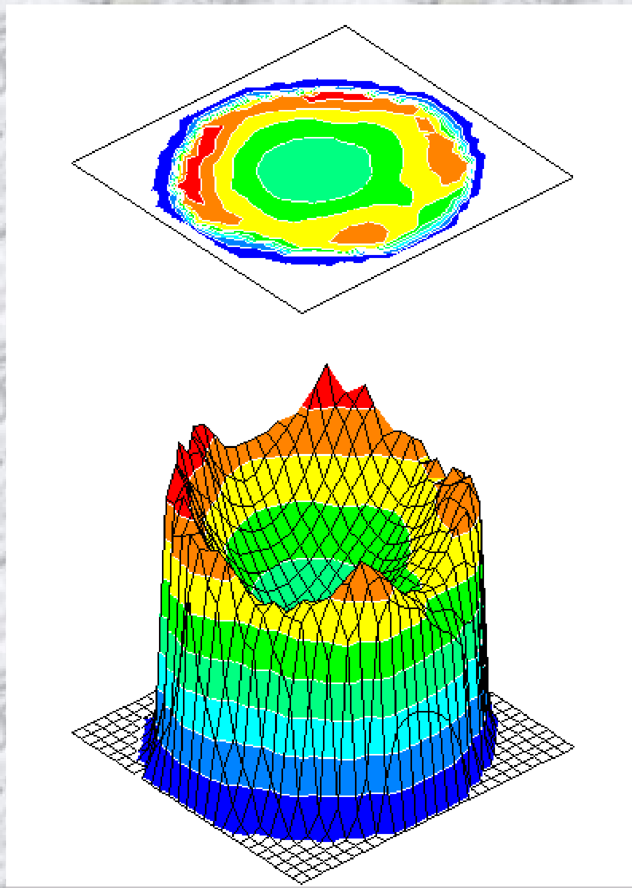

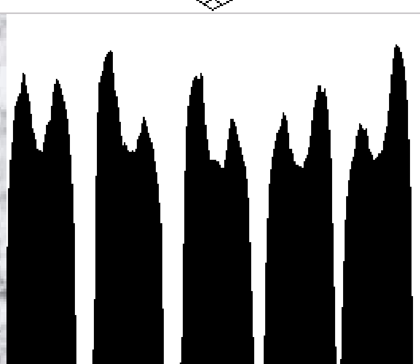

Cs-137 - Failed Rod

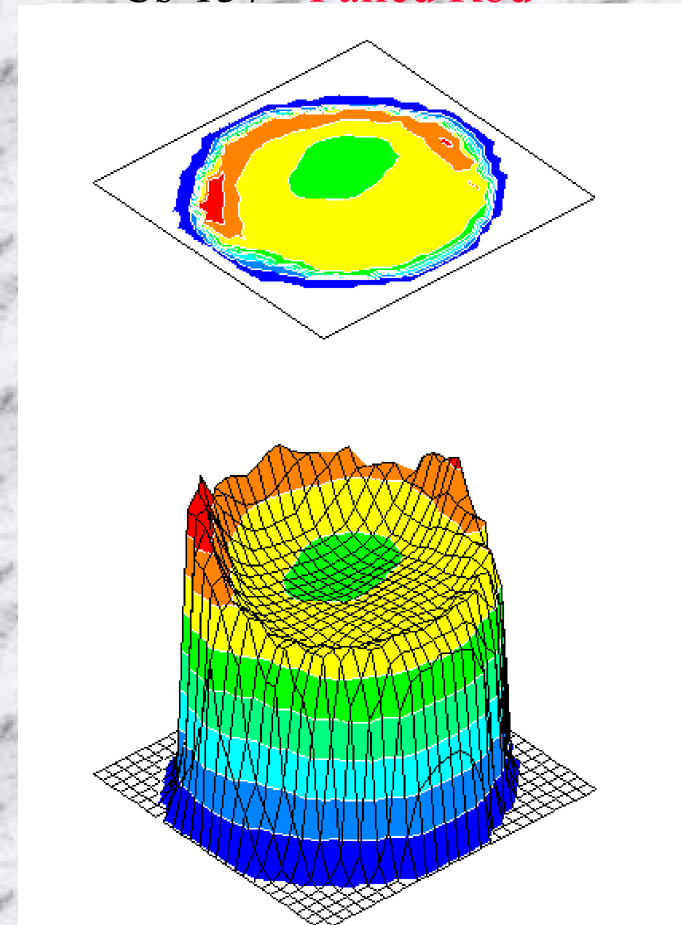

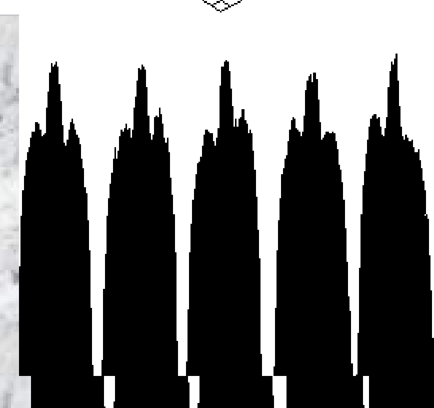

25 x 25 pixels

slit width = 0.25 mm

projection angles = 5

Radial Profiles

Current projects

FEMaS (FP7)

CFC-JET/ITER

Tomo-Analytic

CT Metrology

CT Mobile (FP7)

CERN CT

PCB manufacturing

http://tomography.inflpr.ro

I. Tiseanu, T. Craciunescu, *Assessment of the Aplicability of X-Ray Tomography for Irradiated Samples*, submitted to Fusion Engineering and Design (in press)

I. Tiseanu, T. Craciunescu, G. V. Aldica, M. Iovea, *X-ray micro-tomography as a tool for quantitative characterization of advanced materials manufacturing pro*
. Advanced Materials Research, 47-50, pp. 698-701, 2008.

I. Tiseanu, T. Craciunescu, P. Badica, G.V. Aldica, M. Rindfleisch , Characterization of Superconducting Wires by Cone-Beam Micro-Tomography, acceptata pentru prezentare la IEEE 2008 Workshop on X-Ray Micro Imaging of Materials, Devices, and Organisms, 22-24 October 2008 Dresden, Germany

Gh.V. Aldica, P. Nita, I. Tiseanu, T. Craciunescu, P. Badica, *High Density MgB2 Superconductor: Structure and Morphology through Microtomography and SEM Investigations*, submitted to Journal of Optoelectronics and Advanced Materials

T. Kai, N. Okada, M. Baba, T. Takahashi, M. Misawa, I. Tiseanu, N. Ichikawa, *Structure of effective catalyst layers around bubbles in a fluidized catalyst bed,* Chemical Engineering Journal 130(2007)119-124.

I. Tiseanu, T. Craciunescu, T. Petrisor, A. della Corte. *3D X-ray micro-tomography for modeling of NB3SN multifilamentary superconducting wires*. Fusion Engineering and Design, 82, p. 1447-1453, 2007.

I. Tiseanu, M. Simon, T. Craciunescu, B. N. Mandache, Volker Heinzel c, E. Stratmanns, S. P. Simakov, D. Leichtle. *Assessment of the structural integrity of a prototypical instrumented IFMIF high flux test module rig by fully 3D X-ray microtomography.* Fusion Engineering and Design, 82, p. 2608-2614, 2007.

HM. Prasser, M. Misawa, I. Tiseanu, *Comparison between wire-mesh sensor and ultra-fast X-ray tomograph for an air-water flow in a vertical pipe*, FLOW MEASUREMENT AND INSTRUMENTATION, APR-JUN, 2005,VL 16, IS 2-3, BP 73, EP 83

T. Kai, M. Misawa, T. Takahashi, I .Tiseanu, N. Ichikawa, *Observation of 3-D Structure of Bubbles in a Fluidized Catalyst Bed*, Can. J. Chem. Eng., 2005, VL 83, pp 113-118

I. Tiseanu, T. Craciunescu, B. N. Mandache, O. G. Duliu. *Micro-X-Ray Computer Axial Tomography Application in Life Sciences*. Journal of Optoelectronics and Advanced Materials, 7-2, pp. 1073-1078, 2005.

I. Tiseanu , T. Craciunescu, B. N. Mandache. *Non-Destructive Analysis of Miniaturized Fusion Materials Samples and Irradiation Capsules by X-ray Micro-Tomography.* Fusion Engineering and Design, 75-79, pp. 1055-1059, 2005.

M. Misawa, I. Tiseanu, R. Hirashima, K. Koizumi, Y. Ikeda, *Oblique View Cone Beam Tomography for Inspection of Flat-Shape Objects, Key Engineering Materials*, Advances in Nondestructive Evaluation, Vol 270-273, (2004), pp 1135-1141

T. Craciunescu. *A Neural Network Model for the Tomographic Analysis of Irradiated Nuclear Fuel Rods*. Nuclear Technology, 146-1, pp. 65-71, 2004.

M. Misawa, I. Tiseanu, H.-M. Prasser, N. Ichikawa, M. Akai, *Ultra-fast x-ray tomography for multi-phase flow interface dynamic studies*, Kerntechnik 68 (2003) 3, pp. 85-90

V. Heinzel, P. Bem, E. Esposito, S. Gordeev, U. Fischer, A. Moeslang, S. Simakov, A. Shimizu, M. Sugimoto, I. Tiseanu, P. Vladimirov, Y. Watanabe, T. Yutani, Overview on the IFMIF test cell development, Journal of Nuclear Materials, Vol. 329-333, iss. 2001, pg. 223-227, August 2004, 1.179(2003)

T. Ueda, T. Kai, T. Takahashi, M. Misawa, I. Tiseanu, N. Ichikawa, *Analysis of bubble behaviour in a 3D fluidized bed by fast X-ray CT scanner*, Journal of Chemical Engineering of Japan, 29-1, 2003/01, pp. 112-117

I Tiseanu and team, EFDA Fusion Newsletter, *3-D X-ray Microtomography at MEC Romania*, Vol. 2003/6, December 15, 2003

C. O. Turcanu, T. Craciunescu. *A Genetic Approach to Limited Data Tomographic Reconstructions* Pattern Recognition Letters, 23-8, pp. 967-976, 2002.

M. Misawa, N. Ichikawa, M. Akai, Y. Tomita, Y. Shirayanagi, T. Kawai, I. Tiseanu, T. Kai, *Development of CdTe Line Sensors for Fast X-ray CT Scanner,* J. Radiation Research, Vol 27, No 2, 29-39 (2001)

T. Kai , M. Misawa , T. Takahashi , I. Tiseanu, N. Ichikawa, N. Takada, *Application of Fast X-ray CT Scanner to Visualization of Bubbles in Fluidized Bed*, Journal of Chemical Engineering of Japan, 33-6(2000), pp 906-909.

PCB manufacturing

X-ray tomography

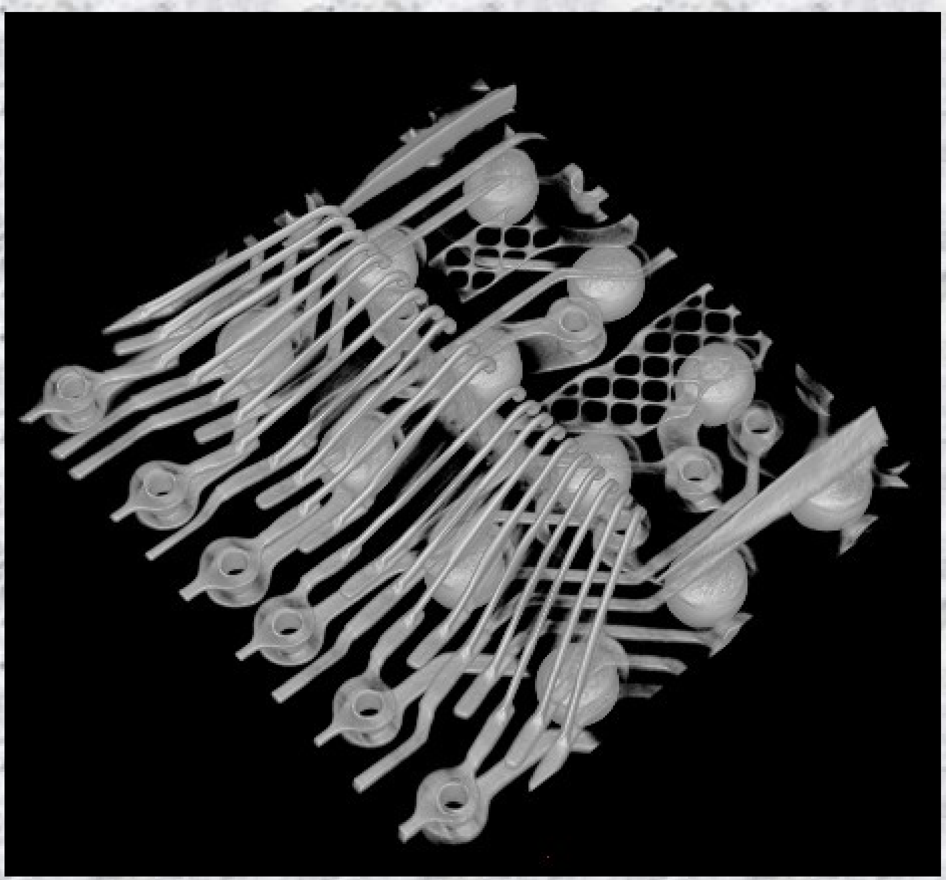

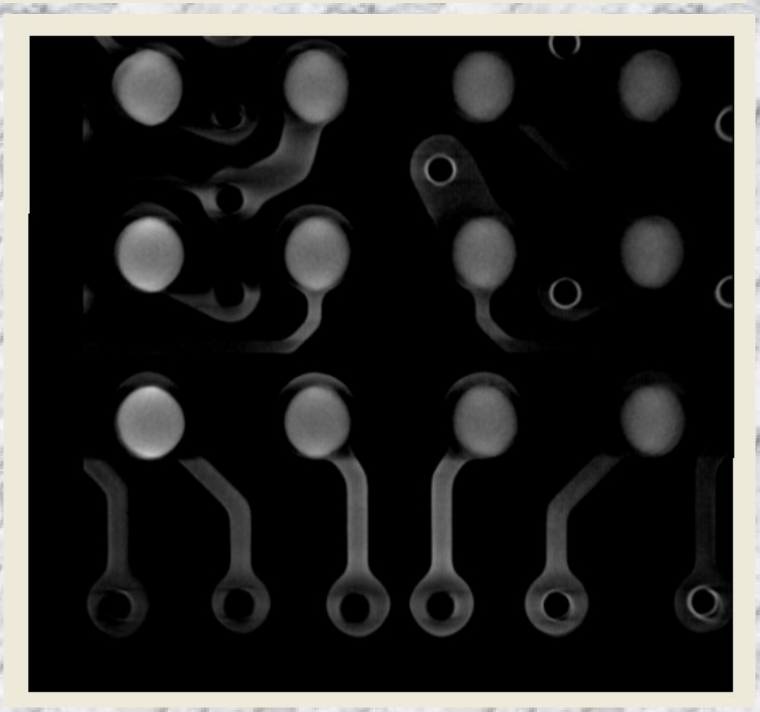

Flip chip bonded solder ball (Pb-Sn), with 10 micron fracture by thermal stress

Facility **Spring-8, Oblique View Parallel Beam**
X-ray energy 29keV
Detector CCD, 2000x1312 pixels
Pixel size 0.47 micron meter equivalent, optical magnification x20 after scintillator (actual magnification x23.6)
Views 360 deg., 1.0 deg steps (0.05 deg. step data available)
Image format 16bit TIFF, no compression
Tomography angle 70deg. (60deg. data available)

Experimental setup

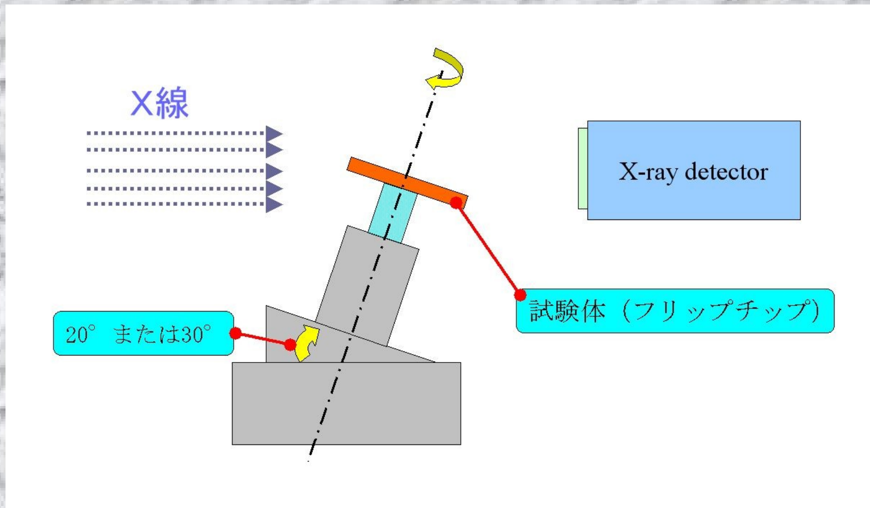

2000x1312 pixels input images
Reconstruction 1200x1200x201
0.47 µm voxel size

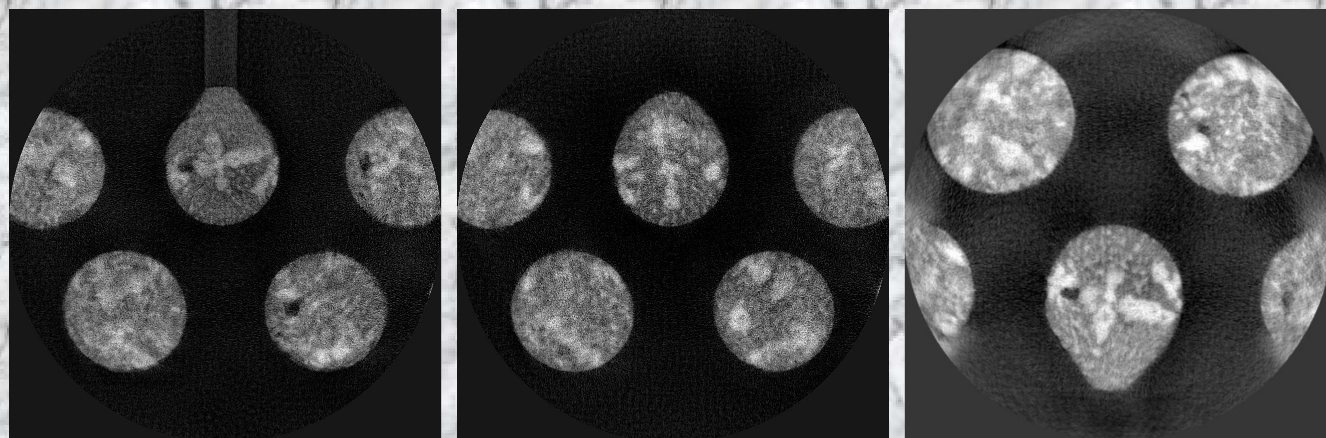

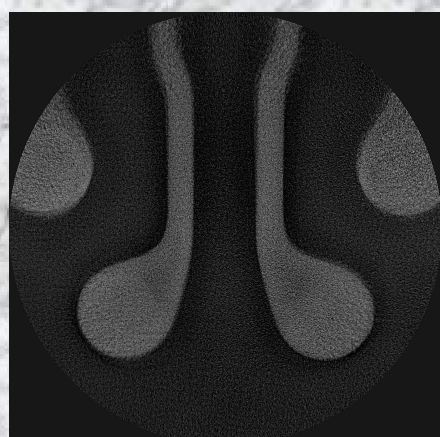

One can see the biased distribution of Pb phase in Sn balls

Computer-aided tomography (μCAT)

μCAT systems are configured to take many views of the object in order to build a 3-D model of its internal structure. 2-D slices through this volume can be viewed as images, or the 3-D volume may be rendered, sliced, and measured directly.

For the NDT inspection of miniaturized samples the microtomography analysis is guaranteed for feature recognition down to a few tens of microns. 3-D tomographic reconstructions are obtained by a proprietary highly optimized computer code based on a modified Feldkamp algorithm.

The microbeam fluorescence (μXRF)

component is a configurable film thickness and composition measuring tool. It include mechanical or optical X-ray beam collimation options, Amptek PIN diode X-ray detector and analysis software, motorized micrometric x-y-z stage for accurate sample positioning. A visual image of the sample is synchronized with the μXRF scanning in order to pinpoint measurement location, as well as for historical documentation.

Overall performances

Microtomography

Spatial Resolution ≅ 20µm
Density Resolution > 1 %
Probe Dimensions:
Diameter < 40 mm, Height < 200 mm
Reconstruction time ≅ 5 min

Microfluorescence

Spatial Resolution ≅ 20µm
Thickness Resolution ≅ 2 % of total layer
Probe Dimensions: 100x100 mm^2

2D composition mapping by micro-beam fluorescence

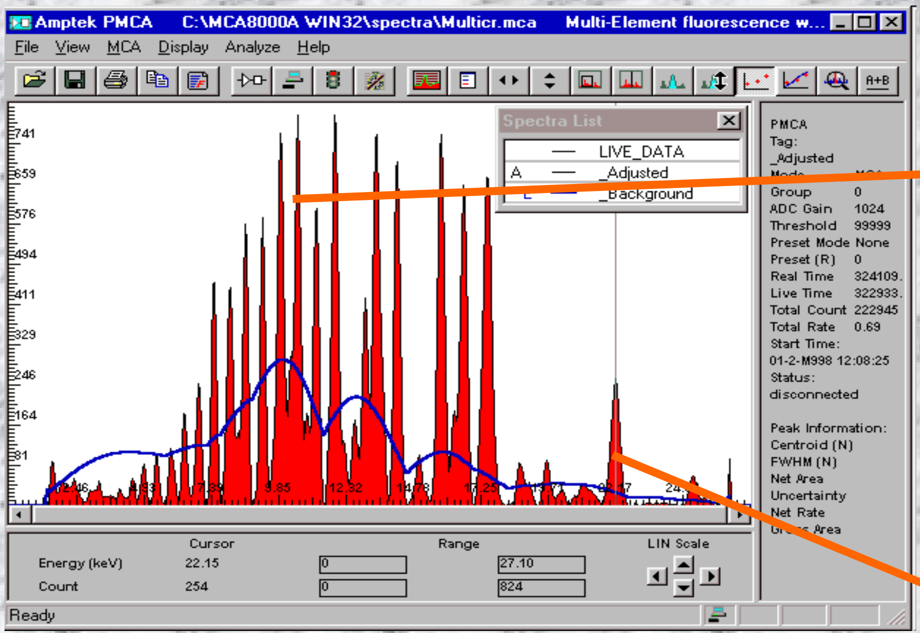

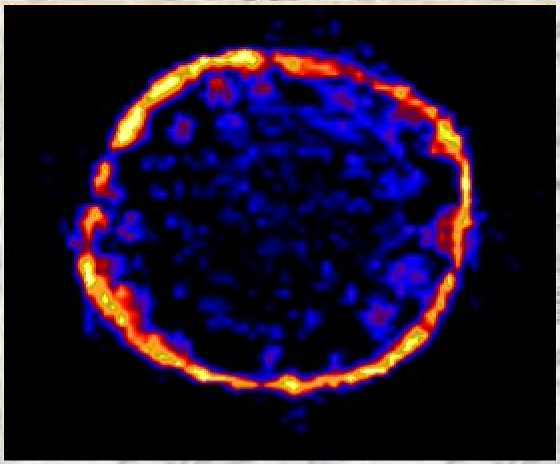

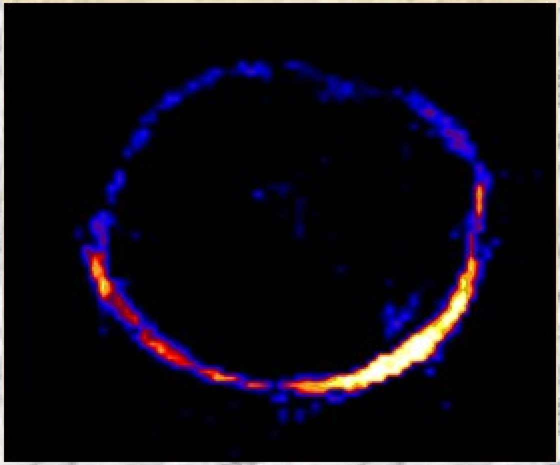

The XRF analysis with fundamental parameters converts elemental peak intensities to elemental concentrations and/or film thicknesses - this enable composition mapping

Radiography and Tomography results for JET CFC samples

CFC-EK386

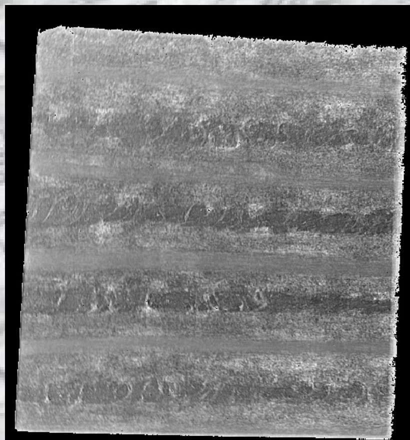

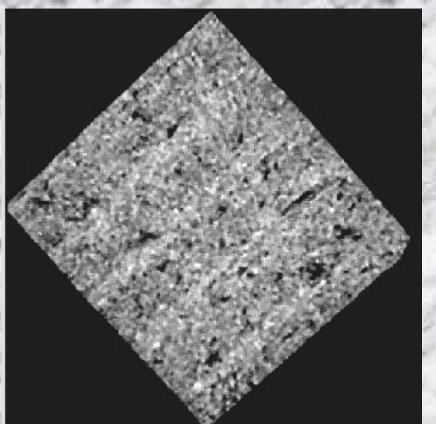

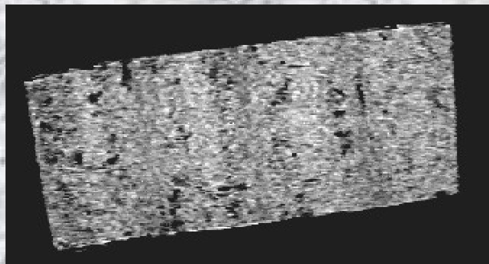

Graphite

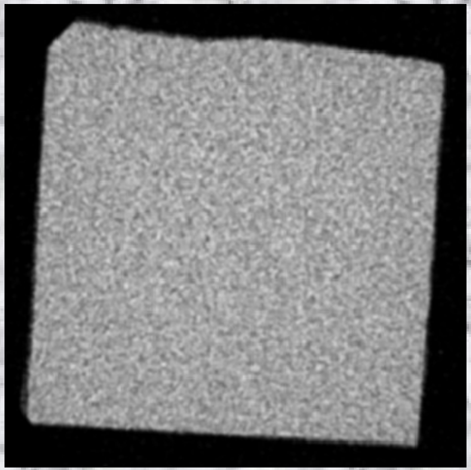

CFC-NB31

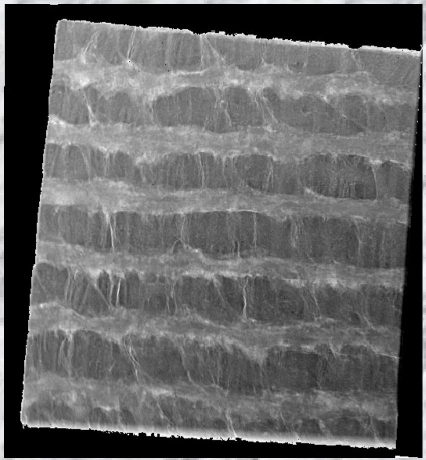

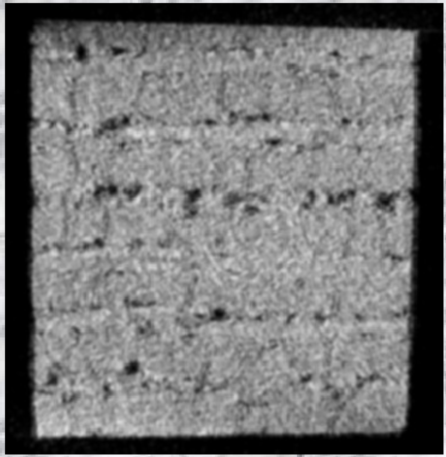

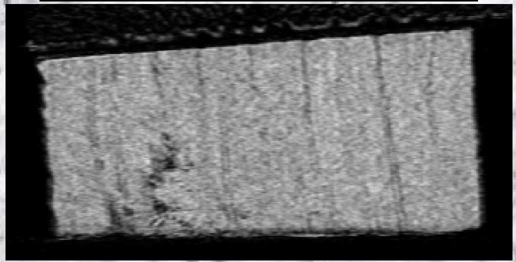

Reconstruction of a *Sepia* cuttlebone

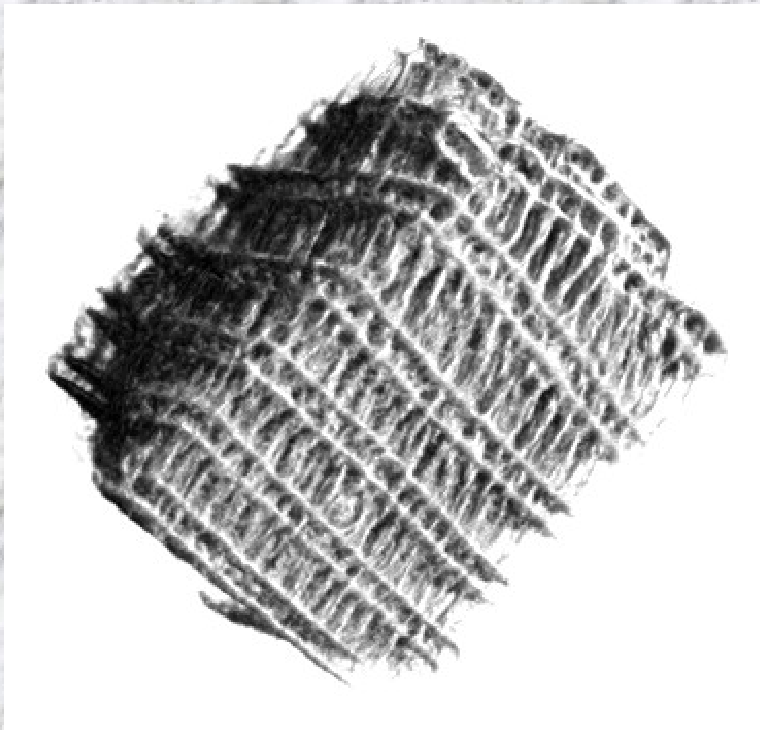

Structural elements – septal thickness, pillar spacing and chamber height in the range of 5 ÷200 µm